MEDICAL PHYSICS PUBLISHING

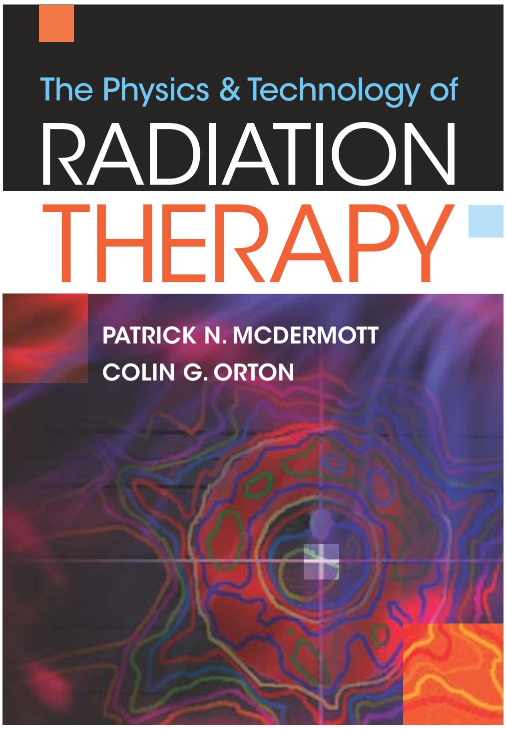

Here is a sample chapter from this book.

Contents

Chapter 3 Atomic Nuclei and Radioactivity

Chapter 4 X-Ray Production I: Technology

Chapter 5 X-Ray Production II: Basic Physics and Properties of Resulting X-Rays

Chapter 8 Radiation Detection and Measurement

Chapter 9 External Beam Radiation Therapy Units

Chapter 10 Central Axis Dose Distribution

Chapter 11 Calibration of Megavoltage Photon Beams

Chapter 12 Calculation of Monitor Unit/Timer Setting for Open Fields

Chapter 13 Shaped Fields

Chapter 14 Dose Distributions in Two and Three Dimensions

Chapter 15 Electron Beam Dosimetry

Chapter 16 Brachytherapy

Chapter 17 Radiation Protection

Chapter 18 Physical Quality Assurance and Patient Safety

Preface

This book is the outgrowth of a course taught to residents in radiation oncology at Wayne State University and at William Beaumont Hospital. Over the years the residents have repeatedly urged that the lecture notes for the course be turned into a book. This is a result of frustration stemming from the lack of a text that is set at the correct mathematical level, is technically accurate, and pedagogically effective.

This book is aimed at the reader who has taken one year of college physics, perhaps years ago (and may not have been terribly thrilled about it). The reader may or may not have taken college calculus or precalculus years ago and may only dimly recall natural logs and the exponential function.

There are a number of excellent texts on the physics of radiation therapy including those by Khan and Johns and Cunningham. We recommend these as good secondary texts for those who wish to go beyond the basics. Both of these texts seem to be a compromise between the needs of graduate students in medical physics and the rest of the radiation therapy community. This book is specifically for the rest of the radiation therapy community. This includes radiation therapy technologists and dosimetrists as well as radiation oncologists; however, it may also be useful to the novice physicist who is looking for a quick qualitative overview. Do not be misled, however; this is not a "watered down" text. Every effort has been made to make explanations clear and simple without *oversimplifying*. If you seek erudite and obfuscating verbiage, find another text. To get the most out of this book we suggest that you "work" your way through it: follow along with pen in hand and work through the example problems and derivations with us (see the quote, page vi).

We are mindful of the fact that people have professional exams that they must study for and pass. This book has been written with a close eye on the requirements for these exams—the ABR boards for physicians, the CMD exam for dosimetrists, and the ARRT for therapists. We make no apology to purists for this. If these exams are good exams, then they reflect what practitioners really need to know to be effective clinicians. Teaching for the exam is simply teaching what people need to know.

It is one of the goals of this book to be interesting so that you will want to read it. We have attempted to accomplish this in two ways: by making the material as directly relevant to clinical activity as possible and by adding some interesting sidelights here and there, such as a brief discussion of atomic bombs, the discovery of x rays, and grand unified theories (GUTS) of particle physics, to name a few. You will have to be the judge as to whether we have succeeded in this.

Whenever possible we have endeavored to explain where results come from and to emphasize principles. In some cases this means simple derivations, in other cases plausibility arguments. Otherwise one is left to blindly memorize facts and rules. Simple memorization leaves one lost when the circumstances change slightly. On the other hand, we don't want this book to be overly "theoretical." For this reason we have included the "clinical example" boxes and "rules of thumb" in the chapters that are more theoretical.

There has not been any attempt to cover treatment planning. It is "beyond the scope of this book," as they say. We recommend the excellent books by Bentel and Khan et al. We do however explain some of the basic principles that determine dose distributions in patients. It is our opinion that the basic foundational material in this book should be covered first, before learning treatment planning.

A word about the use of mathematical symbols and equations. We know that the rather extensive use of mathematical symbols may be foreign to our readers (unless they have majored in mathematics, physics, engineering, or Greek). We have endeavored to choose symbols very carefully for the many quantities referred to in this book. We have tried to make these symbols as simple as possible. As a result of the large number of quantities involved in the study of radiation therapy physics, there are simply not enough Latin letters and we resort to Greek letters and or subscripts. We have tried to conform to standard usage where we believe it to be sensible. Unfortunately there are some symbols that are used for more than one quantity even in standard usage. The meaning of duplicate symbols is generally clear from the context.

Each chapter has a complete summary and a full problem set. Answers to selected problems may be found in appendix D. Clinically realistic dosimetry data for a fictitious linear accelerator may be found in appendix C.

We have made every effort to provide accurate data and information; however the information in this book should not be used for treating patients without first consulting a qualified medical physicist.

We welcome your comments and suggestions. We will try to answer e-mail questions whenever possible.

Patrick N. McDermott, Ph.D.
Email: Patrick.McDermott@beaumonthospitals.com

Colin G. Orton, Ph.D.
Email: ortonc@comcast.net

19 Imaging in Radiation Therapy

19.1 Introduction

The improvement in non-invasive imaging of the human body over the last 35 years has been nothing short of astonishing.[1] The imaging needs of radiation therapy are often quite different from those of diagnostic radiology and can be divided into two broad categories: imaging for treatment planning and imaging for treatment verification. Both of these categories are complex and we can only address the main features here.

Imaging for treatment planning is used to define the gross tumor volume and organs at risk and to select geometric parameters such as the location of the isocenter and treatment beam angles. The imaging modalities used for treatment planning can be divided into two categories: conventional and three-dimensional. Conventional imaging

[1] See *Naked to the Bone: Medical Imaging in the Twentieth Century* by B. Kevles, 1997.

includes general radiography and fluoroscopy. Conventional treatment simulators (see section 19.3) provide these capabilities. Conventional imaging can be thought of as two-dimensional imaging in which three-dimensional anatomy is projected onto a plane. Plane film radiographs are "shadow pictures" or projection images. Three-dimensional imaging modalities include CT (computed tomography), MRI (magnetic resonance imaging), ultrasound, SPECT (single photon emission computed tomography), and PET (positron emission tomography). These modalities provide true three-dimensional anatomical information and in the case of SPECT and PET, metabolic information.

Plane film, fluoroscopy, and CT are based on x-rays as the imaging agent. MRI is based on nuclear magnetic resonance (NMR). It involves "interrogating" the magnetic properties of atomic nuclei in a magnetic field. Radio frequency electromagnetic waves are used to accomplish this. *No ionizing radiation is employed in MRI*. There is an "urban legend" regarding the name "magnetic resonance imaging." The original name for this technique was nuclear magnetic resonance. As the public is so averse to anything with the word "nuclear" in it, the name was changed to MRI. Ultrasound (US) imaging is based on the propagation and reflection properties of sound at tissue interfaces. PET imaging is based on the administration of a positron emitter and the differential uptake of the radiopharmaceutical in different organs and tissues.

For treatment planning purposes it is often necessary to be able to discriminate between various types of soft tissue. Ordinary or "plane" radiographs can distinguish between soft tissue and bone and between soft tissue and air, but not between different types of soft tissue. Generally you cannot see tumors on plane films.

The three most widely used modalities for soft tissue imaging are CT, MRI, and ultrasound. For high spatial resolution and soft tissue discrimination MRI is unsurpassed (see Figure 19.1).

The imaging that we have described so far is *anatomical imaging*. *Functional imaging* such as PET and fMRI (functional MRI) display physiological activity such as glucose metabolism. This promises to play an increasingly important role in the future of radiation therapy.

Traditionally, megavoltage imaging using the treatment beam has been employed for treatment verification using either film or electronic portal imaging devices (EPIDs). EPIDs have now replaced film in most clinics. A new development is image-guided radiation therapy (IGRT). In IGRT the patient is imaged on the treatment machine just prior to treatment. The location of the target is compared with the expected location and the patient is moved to bring the target into alignment with its expected location. A variety of imaging modalities are in use for IGRT including on-board kVp imagers and ultrasound.

Figure 19.1: Side-by-side images of the same axial section made with CT (a) and MRI (b). The superior soft-tissue discrimination of MRI is evident. CT shows bone better than MRI. Note that it is conventional to always display the patient's right on the left-hand side (patients are viewed from inferior to superior direction).

19.2 Digital Images

Digital images are images that can be stored in a computer in numerical form. CT and MRI produce digital images directly. Ordinary radiographic film produces analog images. Film images can be "digitized" by scanning them with a film scanner such as the one shown in Figure 8.24 in chapter 8.

Electronic computers are fundamentally based on a large number of switches. Physically these switches are transistors that reside on integrated circuits ("chips"). A switch may be either "on" or "off." There is no in-between state. An on or off state is like a "yes" or a "no" or like a 1 or 0. For this reason the natural number system for electronic digital computers consists of the digits 0 and 1 only. This system of numbers consisting of only two digits is called base 2 or binary. Our commonly used number system, the decimal system, is base 10. It consists of the digits 0, 1, 2, . . . , 9. The term "bit" is shorthand nomenclature for a binary digit. It is either a 1 or a 0; it is the most elementary unit of information.

Any base 10 number can be expressed as a binary number. Table 19.1 shows the conversion from decimal to binary for the decimal numbers 0 through 5.

A byte is 8 bits of information. An example is the 8-bit number 11000010.

Table 19.1: Binary Numbers

Decimal (base 10)	Binary (base 2)
0	0
1	1
2	$10 = \underline{1} \times 2^1 + \underline{0} \times 2^0$
3	$11 = \underline{1} \times 2^1 + \underline{1} \times 2^0$
4	$100 = \underline{1} \times 2^2 + \underline{0} \times 2^1 + \underline{0} \times 2^0$
5	$101 = \underline{1} \times 2^2 + \underline{0} \times 2^1 + \underline{1} \times 2^0$

Alphanumeric characters are the 26 letters of the alphabet (both upper and lower case) plus the ten base ten digits 0, 1, . . . , 9 and special symbols such as $, #, etc. A byte can be used to represent a particular alphanumeric character. There are 2^8 different ways to represent a string of 8 ones and zeroes. Therefore there are $2^8 = 256$ possible characters a byte can represent. This is the reason that the original PC character set contains 256 characters.

There are some useful prefixes in computer science that are a little different (we won't make a bad pun and say "a bit different") than defined in Table 2.2. A kilobyte is $2^{10} = 1024$ bytes. A megabyte (MB) is $2^{20} = 1{,}048{,}576$ bytes. A gigabyte is 2^{30} bytes, etc. As an example, a 100 GB storage disk will hold approximately 1.074×10^{11} bytes of data.

There is a standard binary coding scheme for alphanumeric characters, the <u>A</u>merican <u>S</u>tandard <u>C</u>ode for <u>I</u>nformation <u>I</u>nterchange, known as *ASCII* (pronounced ass-key) for short. There are 128 standard characters and each character is represented by an 8-bit (one byte) number. For example a "W" is represented as the 8-bit binary number 01010111. ASCII is the *lingua franca* of the computer world. Most computers recognize ASCII. A page of ASCII text is about 2 kbytes. A more recent industry standard is Unicode, which is used to represent about 100,000 different text characters in use throughout the world.

Digital images are divided up into an array or grid of <u>*pic*</u>ture <u>*el*</u>ements called *pixels*. The pixel size influences the spatial resolution of an image. The larger the pixel size the poorer the resolution (see Figure 19.2). For a specific image, smaller pixel size means that more pixels are necessary to depict the entire image. More pixels provide higher spatial resolution. There is a cost however; more pixels mean more storage space required. Radiological images are generally either 512×512 pixels or 1024×1024 pixels. This is crude compared to the resolution available in consumer digital cameras.[2]

[2] At the time of this writing, 10 megapixel cameras are common. This corresponds to an image of 3888×2592 pixels.

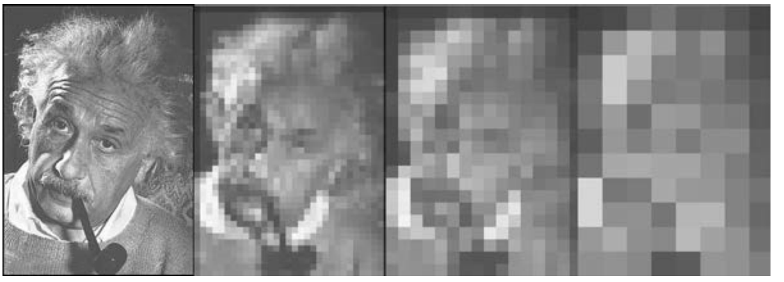

Figure 19.2: A series of four images with different numbers of pixels. The first image on the left has 345×487 pixels. The second image is approximately 30×45 pixels. The third is approximately 16×22 and the fourth is 8×11. The larger the number of pixels, the greater the spatial resolution.

Example 19.1

The field of view of a fluoroscopic unit is 9 in. (23 cm) across. Images are acquired in a 512×512 pixel format.

What is the pixel size and what is the size of the smallest object that can be resolved?

The pixel size is 23 cm/512 = 0.45 mm per pixel. Any object that is about 0.5 mm or smaller will be difficult to discern.

Images that we might normally describe as "black and white" (such as in old movies) actually have many shades of gray. In a "gray scale" image, each pixel is assigned a number that represents a shade of gray or a gray level. This is called the gray scale. In a color image each pixel is assigned a number that represents a color. The numerical values assigned to a pixel are binary. An example is an 8-bit gray scale which has $2^8 = 256$ shades of gray. The number of shades of gray in an image affects the *contrast* resolution of the image. This is illustrated in Figure 19.3.

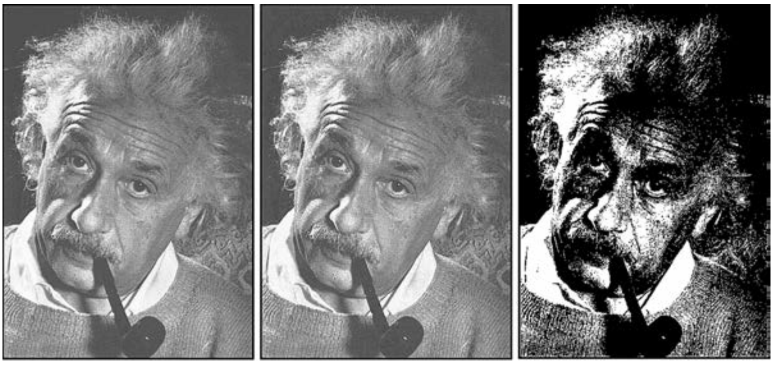

Figure 19.3: Three images having different gray-scale levels. The image on the left has an 8-bit gray scale. The middle image has a 4-bit gray scale. The image on the right is a 2-bit image: there are only two shades—black and white. This image is true black and white.

Example 19.2

A CT image is 512×512 pixels and has 16-bit pixel values (only 12 bits are used for the gray scale). How many bytes are required to store this image?

The total number of bits = 512×512×16 = 4,194,304 bits. The number of bytes = 4,194,304/8 = 524,288 and 524,288/1024 = 512 kbytes. The file will be slightly larger because of the presence of an image "header" containing information about the image (patient name, date, etc.).

For three-dimensional imaging purposes the region of interest in a patient is divided up into a large number of small volume elements or voxels. The goal of three-dimensional imaging is to determine the value of some quantity characterizing the tissue in each one of the voxels. This value is presumed to be constant within each of the small voxels. The image can only be displayed however in two dimensions as either a sectional image or a projection image.[3] A sectional image is often described as a "slice." A slice may be as little as one voxel thick. There are three principal types of sectional images. An axial or transverse slice divides a patient into two halves, a superior half and inferior half.

[3] This paragraph follows the discussion in *Radiation Oncology: A Physicist's Eye View* by M. Goitein, 2008.

A coronal section divides a patient into an anterior half and a posterior half and a sagittal section divides a patient into left and right halves. A projection image is one in which each pixel represents a transmission value through all tissue traversed between the source and image plane. The prime example is an ordinary radiograph.

Standardization of image data files is a very critical issue. It is important to be able to seamlessly transfer images between imaging devices, treatment planning systems, record and verify systems, etc. Most manufacturers now comply with the DICOM (Digital Imaging and Communication in Medicine) standard. An extension of this standard is called DICOM-RT and includes specific provisions for radiation therapy. Radiological images are often stored and transferred within a *P*icture *A*rchiving and *C*ommunication *S*ystem (*PACS*). This replaces hardcopy film and allows remote access. A PACS consists of servers for image storage that are connected to client viewing stations via a network system. A PACS enables easy access to radiological images anywhere throughout a hospital or hospital system.

19.3 Conventional Simulators

There are two types of simulators used for radiation therapy: conventional and CT. Both types of simulator are intended to provide information necessary for the planning and treatment of patients. A conventional simulator is a device which mechanically simulates the behavior of a linac or Co-60 unit (see Figure 19.4). There is a gantry, which can rotate, and a couch, which may be identical to a linac or Co-60 treatment couch. All of the motions that are possible on a linac are duplicated in a conventional simulator. In addition, the source-axis distance (SAD) can be set on a simulator. Simulators also have a block tray holder. The tray slot must be at the same distance from the x-ray source as the tray on the linac. In addition, a conventional simulator is capable of kV (diagnostic quality) imaging including fluoroscopy. This is needed to assist in planning patient treatments. Linear accelerators are not capable of diagnostic quality images or fluoroscopy. This is the major reason a simulator is used rather than a linac to plan a patient's treatment. Fluoroscopy allows adjustment of the beam position under real time conditions. Conventional simulators are likely to disappear over the next ten years in favor of CT simulators.

A simulator room is divided into two areas: a control console area and an area containing the simulator. The simulator consists of a console, a gantry, a gantry stand, and an x-ray generator. The simulator room is the place where most of the information necessary to plan and to treat a patient is gathered. Once simulation data are collected (films, gantry angles, etc.), it will be passed along to a dosimetrist for treatment planning on a treatment planning computer system. The simulator room has wall-mounted lasers for patient positioning just like a treatment

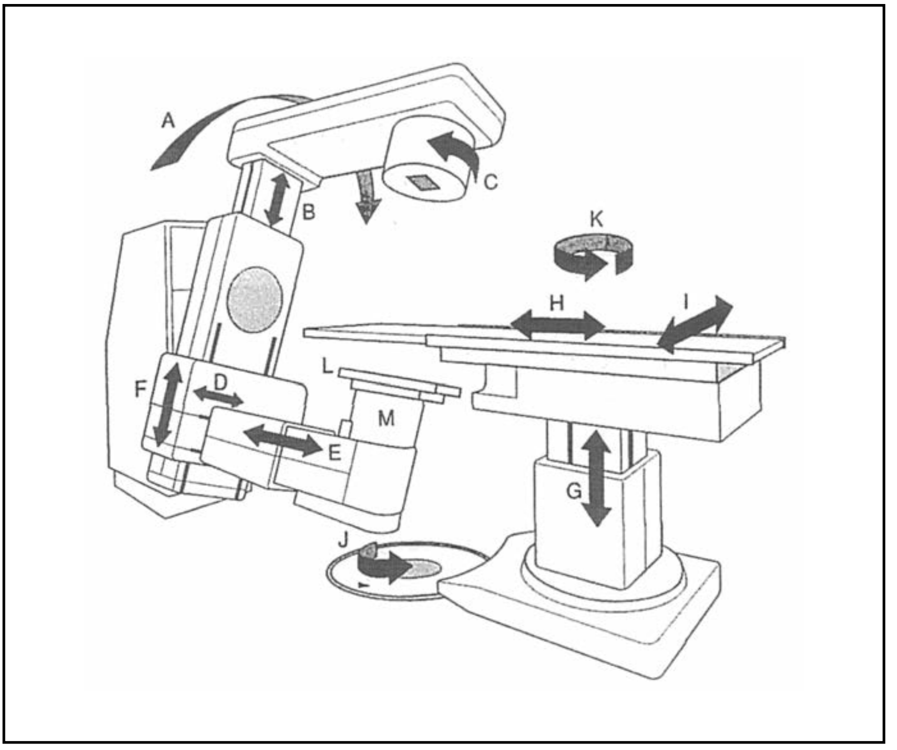

Figure 19.4: A conventional simulator is designed to be mechanically like a linac in that it mimics the motion of a linac. The exception is that the SAD can be changed (B). The head houses a diagnostic x-ray tube and at the other end of the gantry there is a grid, film cassette holder (L), and an image intensifier (M) for fluoroscopy. The image intensifier can be moved laterally (D and E) and up and down (F). (Reproduced from *Radiotherapy Physics in Practice*, J. R. Williams and D. I. Thwaites (eds.), Fig. 7.3, p. 125, © 2000 by permission of Oxford University Press.)

room (see Figure 18.2 in chapter 18). Treatment aids, such as immobilizing devices, are usually fabricated during a patient's simulation appointment. The patient is usually marked or tattooed in the simulator room.

The simulator has a diagnostic x-ray tube in the head, which is used for fluoroscopy and plane film imaging. Focal spot sizes range from 0.4 to 0.6 mm for the small spot and 1.0 to 1.2 mm for the large spot. The simulator has a grid, a film cassette holder, and an image intensifier (II) for fluoroscopic imaging. Newer simulators have digital flat-panel, solid-state detectors instead of an II. Fluoroscopy is activated with the use of a foot pedal. The II can be moved up and down, from side to side, and in and out. The presence of the II constrains gantry and table motion. A collision avoidance system is built into the II so that it cannot hit the treatment couch.

The II is a large, evacuated tube with a cesium iodide fluorescent screen at one end that converts x-rays to light (see Figure 19.5). The light from this screen strikes a photocathode, which in turn emits low-

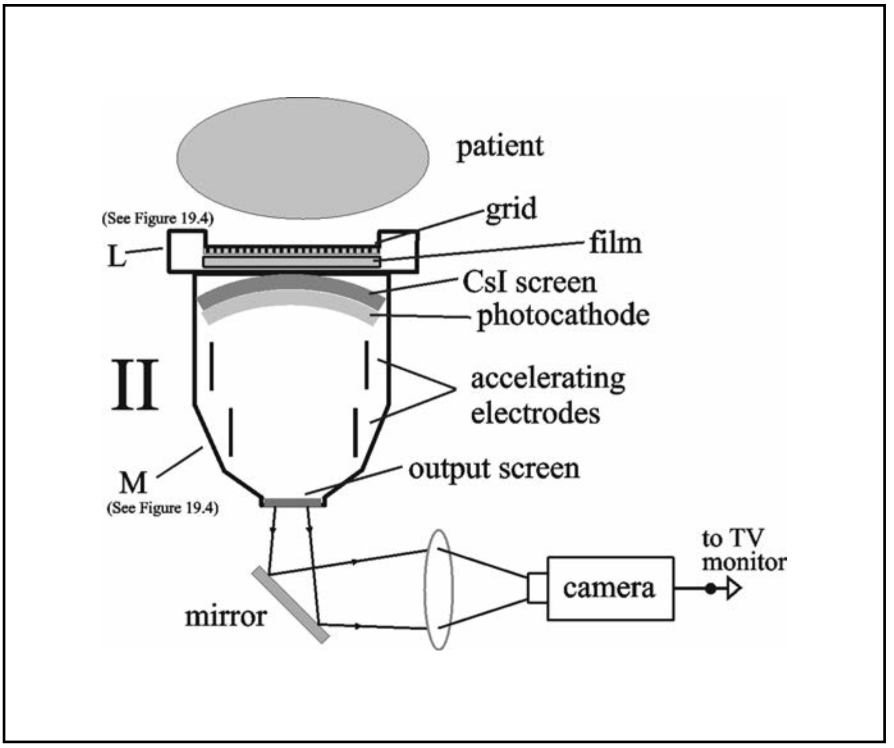

Figure 19.5: An image intensifier (see L and M in Figure 19.4) is a large evacuated tube that contains a fluorescent cesium iodide input screen. The CsI input screen converts x-rays to visible light, which in turn strikes the photocathode and generates electrons. The electrons are accelerated and focused. When the electrons strike the output screen, they produce a smaller and much brighter image.

energy photoelectrons. In this way the x-ray image is converted to an electronic image. The electrons are accelerated and focused by a high voltage (up to 30 kV) between the ends of the tube. At the end of the tube the electrons strike a small output fluorescent screen, producing a visible light image of high brightness. The brightness gain is due to two factors: the energy acquired by the accelerated electrons and the reduction in the diameter (minification) of the image. The image is directed into a camera through a mirror tilted at a 45° angle. The image is viewed on a TV monitor in the control console area. Many simulators have "last image hold," which enables continued viewing of an image after the x-ray beam turns off. The brightness level is set by the automatic brightness control (ABC). A photocell located between the II and the camera sends a signal back to the generator to adjust the kVp or mA. As the patient is moved with respect to the II, the ABC maintains the proper brightness level.

When planning patient treatment it is necessary to select gantry, collimator, and couch (pedestal) angles for each beam or treatment field. In addition, the location of the isocenter must be chosen with respect to

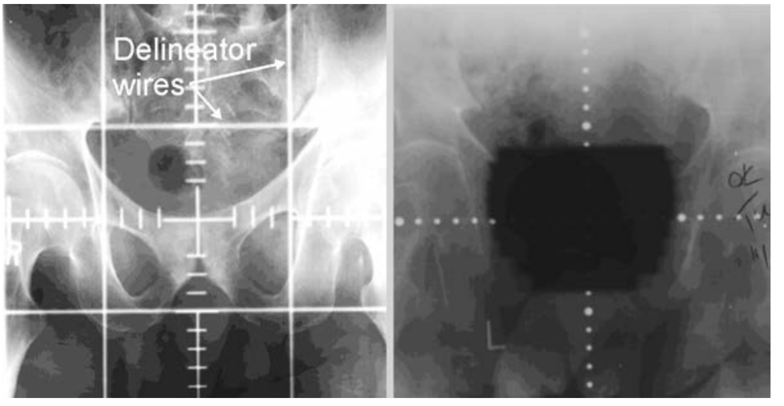

Figure 19.6: A simulation film of a patient's pelvis (a) next to a 6 MV localization film (b). The quality of the simulation film is far superior to the localization film. The delineator wires are shown on the "sim" film. A graticule on the sim film shows lateral distance as measured at isocenter. The wires are set for a 10×10 cm^2 field. The dark central area on the localization film is the treatment field.

the patient. Simulators have four independent delineator wires which take the place of linac independent jaws and cast a shadow which shows where the jaws will be positioned on the linac. This allows the physician to view adjacent anatomical structures. Radiographic contrast agents may be used in the bladder, etc. A graticule scale projected onto the film shows the beam central axis and graduated scale (see Figure 19.6).

The control console is used to set the radiographic technique: kVp, mA, and time. Modern generators produce high-frequency dc with low ripple (see chapter 5, section 5.2). The control console is behind a barrier which is shielded against kV scatter x-rays. There may be an interlock on the exterior door so that the x-ray beam is shut off if the door is opened. The simulator and patient can be viewed from the control console, usually through a leaded glass window. The control console can also be used to remotely set the gantry angle, collimator angle, delineator wires, and position of the II. The control area also has the video display monitor for fluoroscopy.

19.4 Computed Tomography

Computed tomography (CT) was developed by G. N. Hounsfield and A. M. Cormack. The first commercially available unit was introduced by EMI Ltd., in 1970. This company is perhaps best known for first recording the Beatles! Hounsfield and Cormack won the Nobel Prize for

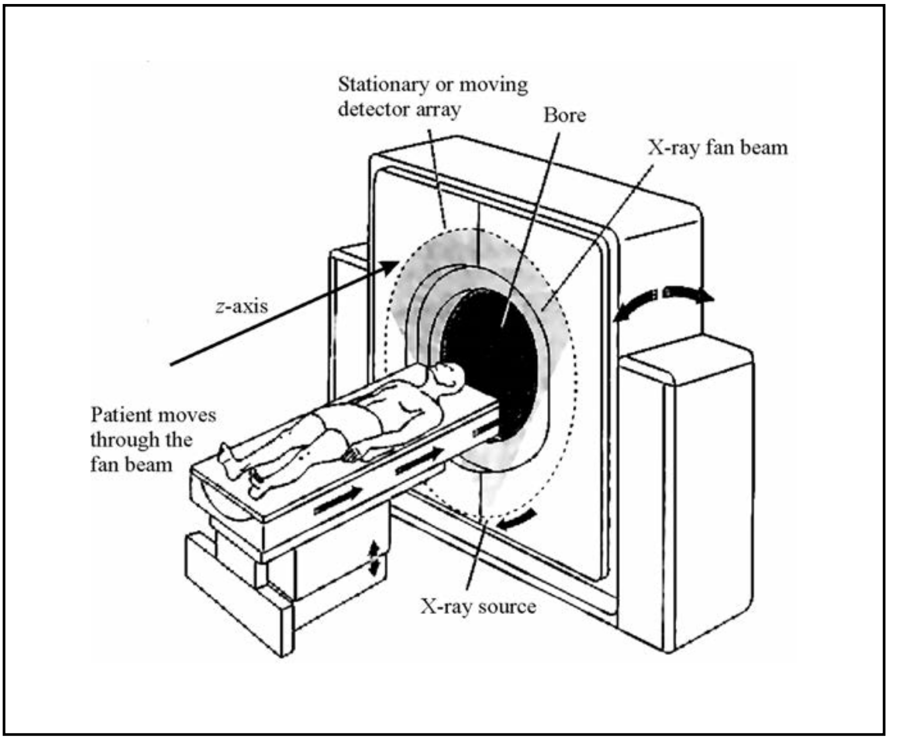

Figure 19.7: The mechanical motions of a CT scanner. The table is moved into the bore. An x-ray tube inside the gantry rotates around the patient. A detector array registers the x-ray intensity passing through the patient. The detector signals are fed to a computer, which then "reconstructs" a series of axial images ("slices") of the patient. (Reproduced from *Radiotherapy Physics in Practice*, J. R. Williams and D. I. Thwaites (eds.), Fig. 7.8, p. 135, © 2000 by permission of Oxford University Press.)

Medicine in 1979. CT was one of the most significant developments in medical imaging in the twentieth century. What's the breakthrough?

(1) Three-dimensional imaging.
(2) Soft tissue discrimination.

Herein lies the power of CT.

As shown in Figure 19.7 the patient lies on a table, which can move up and into the aperture (sometimes called the bore). The inferior and superior scan limits are selected first by performing a transmission scan (also called a topogram, scout, or surview). For this purpose the patient is moved through the bore while the x-ray tube is on but stationary (not rotating). Based on the image formed by this procedure, the operator then selects the inferior and superior limits of the scan. During the scan itself the x-ray tube rotates around the patient. The x-rays pass through the patient and are detected by a detector array opposite the tube and converted into electrical signals. The signals from the array are fed into a computer, which then "reconstructs" an axial slice or tomogram (see Figure 19.1) of the patient. This is quite different from the "shadow" picture formed by plane radiography. As the table moves further into the bore, successive slices in the inferior direction are reconstructed. These slices can be stacked to form a three-dimensional image of the patient. This provides a digital model of the patient, including both geometric data (location of skin surface, tumor, and organs at risk) and composition data (linear attenuation coefficient). This digital model is exported to a treatment planning system.

CT images are the primary imaging modality used for radiation therapy treatment planning purposes. There are three reasons for this: CT images are spatially accurate. They are not subject to spatial or geometric distortions. An accurate model of the patient is necessary for accurate dose calculations, both spatially and in terms of composition (i.e., electron density). The second reason is that the spatial resolution of CT is relatively high (compared to PET, for example). The third reason is that electron density data can be derived from the CT number (CT#), provided that a calibration curve is available (see section 19.4.3). MRI can suffer from spatial distortion, and it does not provide electron density data.

CT images represent a "virtual" patient. CT units are either diagnostic scanners or speciality scanners, called CT simulators, sold specifically for radiation therapy treatment planning. The advent of CT simulators and the use of "virtual simulation" may signal the end of conventional simulators. Virtual simulation involves the use of CT images along with software to "virtually" simulate and plan treatment. The role that CT plays in treatment planning is twofold:

(1) *Contour data:* provides true 3-D data on spatial location of skin, tumor, normal organs and tissues.
(2) *Electron density:* recall that Compton scattering is the dominant photon interaction at megavoltage therapy energies—depends primarily on the electron density (electrons/cm^3) $\Rightarrow$ inhomogeneity corrections depending on electron density.

19.4.1 Development of CT scanners

Early model CT scanners acquired a single axial slice at one time with the table immobile during tube rotation. The x-ray tube generates a fan beam of x-rays that rotates around the patient. The table is then advanced to acquire the next slice. In this way contiguous axial slices are generated. In the early 1990s spiral scanners were developed in which the table moves continuously while the x-ray beam remains on, tracing out a helical path around the patient. At about the same time, multi-slice scanners were introduced. These scanners are capable of acquiring multiple slices simultaneously. We will discuss each of these important developments below.

We begin with a discussion of the development of axial (non-spiral), single slice scanners. These scanners have evolved through four generations as shown in Figure 19.8. The first generation scanners used a pencil beam (Figure 19.8a) and a single detector. Both the x-ray tube and the detector first moved horizontally (translate) through 180 positions and then the x-ray tube and detector rotated 1°. This translate-rotate process was repeated until sufficient projections were obtained to form an image. It is not surprising that scan times were long, about 5 minutes for a single axial slice. Second-generation scanners (Figure 19.8b) used an x-ray fan beam and a multiple linear detector array. These scanners also operated in a translate-rotate mode. The multiple detectors increased speed considerably, but it still took as long as 20 seconds to image a single slice. Third-generation scanners use a fan beam and a detector array containing at least 30 elements (Figure 19.8c). Translation is no longer necessary, and both the tube and detector rotate. Scan times are as low as 1 second for an axial slice. In a third-generation scanner, each detector element images a particular annulus of the patient's anatomy. If an element is not functioning properly, a "ring" artifact may result. In a fourth-generation scanner (Figure 19.8d) the detectors form a ring completely surrounding the patient and therefore only the x-ray tube rotates. Most scanners sold today are actually third-generation scanners.

The x-ray detectors are either xenon gas ionization detectors, used in some third-generation scanners, or solid-state scintillation crystals used in third- and fourth-generation scanners. The thinnest slice thickness is determined by detector collimation and reconstruction parameters. Various slice thickness settings are possible: 1, 2, 5, and 10 mm are common. Spatial resolution can be as good as 0.6 mm in the axial plane.

Single-slice scanners have two major disadvantages. First, they are very slow, and second they suffer from poor resolution in the longitudinal direction. A non-spiral set of single-slice CT scans for treatment planning using a third- or fourth-generation scanner can take as long as 45 minutes. This is time-consuming for staff, and it is difficult for some patients to remain in immobilization devices this long. Practical values of the slice thickness are relatively large. The resolution in the axial plane of a CT image is typically about 1 mm. It is not uncommon with old scanners to use a slice thickness of 5 mm or even 10 mm. The slices are then stacked to form what could be described as a "pseudo 3-D" image. Because the resolution in the longitudinal direction is considerably poorer than in the axial plane, any object or boundary within a given slice will be imaged, but its location within the slice will be

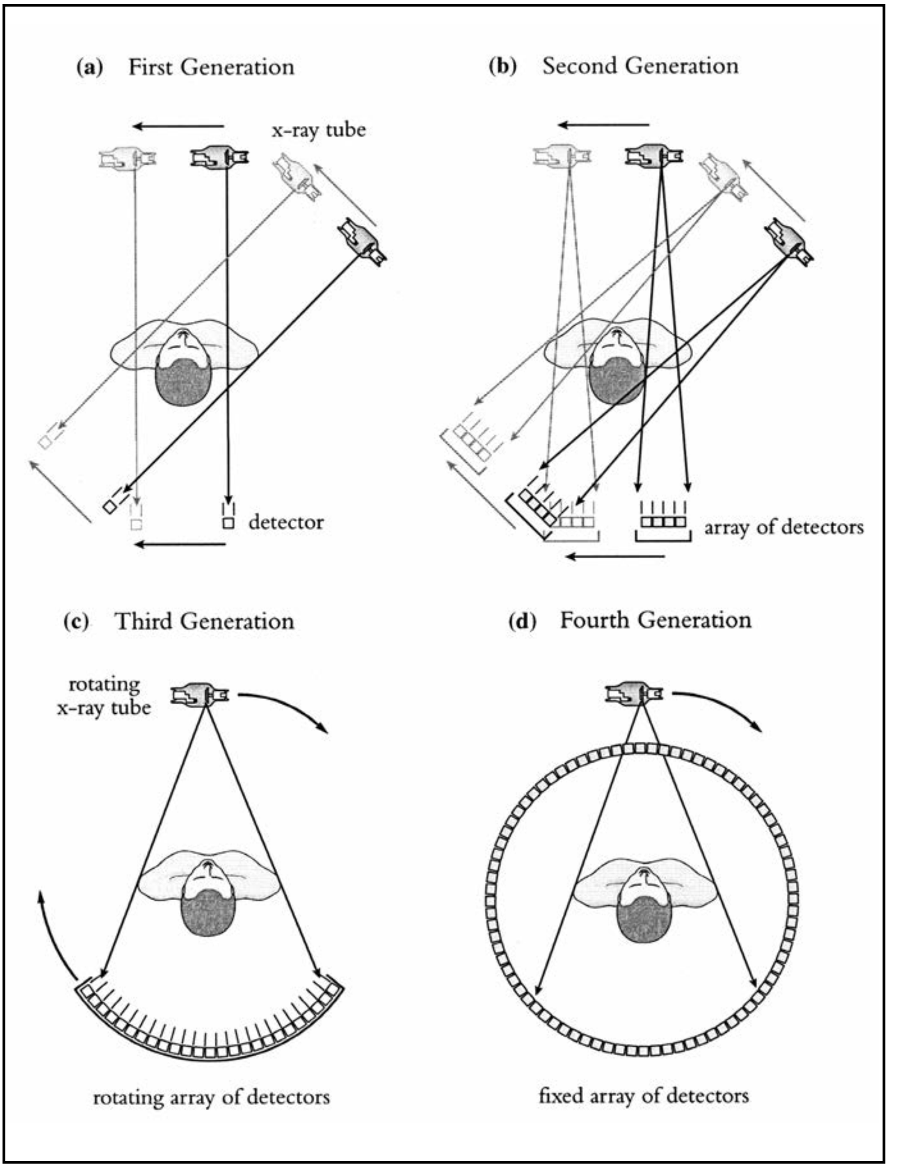

Figure 19.8: The four generations of CT units described in the text. (a) is a first generation unit, (b) is second generation; (c) and (d) are third and fourth generations. Most CT units sold today are third generation. (Reproduced from "CT Basics" by D. Cody in *The Physics and Applications of PET/CT Imaging,* Figs. 1 and 2, pp. 30, 32. © 2008, with permission from American Association of Physicists in Medicine (AAPM); previously printed in "Computed Tomography" by T. G. Flohr, D. D. Cody, and C. H. McCullough in *Advances in Medical Physics: 2006,* A. B. Wolbarst, R. G. Zamenhof, and W. R. Hendee (eds.), Figs. 3-4a/b, p. 63, © 2006, Medical Physics Publishing.)

unknown. This is sometimes called "volume averaging." This implies that the location of anatomical boundaries is uncertain by an amount approximately equal to the slice width. A 10-mm uncertainty in the superior/inferior direction may be unacceptable for highly conformal radiation therapy. In addition, digitally reconstructed radiographs (DRRs, see section 19.4.4) suffer from poor quality when the slice thickness is large.

New CT scanners are now helical (sometimes called spiral) scanners. These were introduced in the early 1990s. A non-spiral scan will be referred to as an axial or sequential scan. Modern CT scanners can acquire images in either axial or spiral mode. Spiral scanners are third generation and as such both the tube and detector rotate. Electrical cables run both to and from the tube and the detector, carrying power and data. In an axial scan the x-ray tube rotates as much as 360° around the patient.

If rotation in an axial scanner were to continue in the same direction past 360°, the cables would become increasingly wound or twisted. Therefore tube rotation must stop to avoid winding up cables. During this time interval, the table is moved (indexed) further into the bore by an amount that is usually equal to the slice thickness and then the next slice is acquired. Spiral CT is based on a continuous rotation of the x-ray tube as the patient is translated through the scanning aperture. Spiral scans eliminate the dead time associated with table motion. In this way it is possible to obtain up to 40 slices in a single breath hold. This reduces motion artifacts. Spiral CT has become possible through the introduction of "slip-ring" technology, which avoids the problem of cable winding. The faster the tube can rotate, the more rapidly a scan can be completed. CT units are now available in which the tube can rotate through 360° in as little as 0.3 seconds. This places severe cooling demands on the x-ray tube and housing. These tubes must be capable of handling a heavy heat load. They are therefore expensive, over $100,000. Oil is pumped through the tube housing and circulated through a radiator. The rapid rotation requires the gantry to be spin balanced like an automobile tire.

Newer CT units are capable of multiple-slice scanning (see Figure 19.9). These units can acquire more than a single slice simultaneously. There are units that can acquire up to 64 slices at one time. These use multiple rows of detectors extending along the longitudinal direction (z-axis, see Figures 19.7 and 19.9). The signals can be combined from adjacent elements to form slice thicknesses that are multiples of the size of a single detector element. The detector elements often have varying width—smaller near $z = 0$. The total scan thickness in a single rotation is related to the entire detector. The x-ray beam is now a cone beam instead of a fan beam. Multi-slice units are third-generation scanners. The advantages of multi-slice scanning are faster acquisition time, reduced tube loading, the option of respiratory gating or sorting,

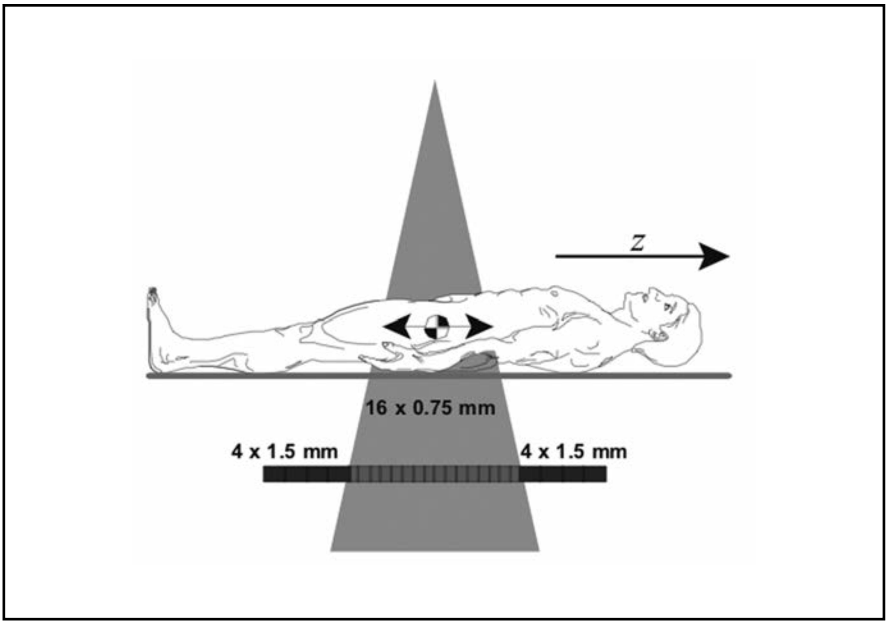

Figure 19.9: A multi-slice CT scanner showing the detector array and the cone beam diverging in the longitudinal direction. A single-slice scanner would have a very narrow (in the longitudinal direction) fan beam whereas a multi-slice scanner has a cone beam. In this illustration the collimator has been set to produce a 16-slice scan; each slice is 0.75 mm thick (all dimensions measured at the isocenter). The largest total scan thickness for this scanner is $16 \times 0.75 + 8 \times 1.5 = 24$ mm.

thinner slices, and greater volume coverage on a single tube rotation. Slice thicknesses of as little as 0.5 mm are feasible. This is true 3-D imaging—the resolution in the *z*-direction is as good as the resolution in the axial plane. Multi-planar reconstruction becomes a useful option; the resolution in coronal and sagittal planes is as good as in an axial plane.

There are some disadvantages of multiple slice scanning. The use of a cone beam as opposed to a fan beam leads to increased scatter in the patient and to the detector. To maintain image quality, scattered photons are partially eliminated by using radiopaque separators (septa) between detector elements in the *z*-direction. This arrangement acts like a grid in a film cassette to eliminate image degradation due to scatter radiation (see chapter 4, section 4.4). The dose is higher for a multi-slice scan compared to an axial scan of like quality. This is due in part to increased scatter in the patient from the large cone beam and decreased efficiency because of the presence of the septa between detector rows.

Each patient may have hundreds or up to perhaps one thousand images (4D CT). As an example of data storage requirements, suppose 100 patients are under treatment at a given time. Let us assume that there are 150 images per patient and each image is 512×512 pixels. Each pixel is 2 bytes (actual gray scale is 12 or 14 bits, they do not use the full 16 bits). This requires 512×512×2×150×100 = 7.3 GB storage just for current patients.

Reconstruction of images from a spiral scan is affected by the distance that the table moves in one revolution of the x-ray tube and by the beam thickness. The quantity pitch has been defined to describe this. With the introduction of multi-slice scanners the definition of pitch has been refined so that it is relevant to both axial and multi-slice scans:

$$P = \frac{\text{Table travel per rotation}\left(\text{mm}\right)}{\text{T}'} \tag{19.1}$$

For a single slice axial scanner T′ is the beam thickness as determined by the x-ray collimator in millimeters. For a multi-slice scanner T′ is the total length of the tissue irradiated in millimeters (the length covered by the beam in Figure 19.9).

The pitch has a direct impact on patient dose and image quality. When $P < 1$ (see Figure 19.10) there is an improvement in image quality, but the dose is increased because of overlapping helical slices. When $P > 1$, less time is required for the scan, but not all regions are fully sampled; some z interpolation may be necessary resulting in a loss of resolution along the z-axis. The pitch values for one commercially available CT simulator range from 0.07 to 1.7 (for 4D CT, see section 19.4.6).

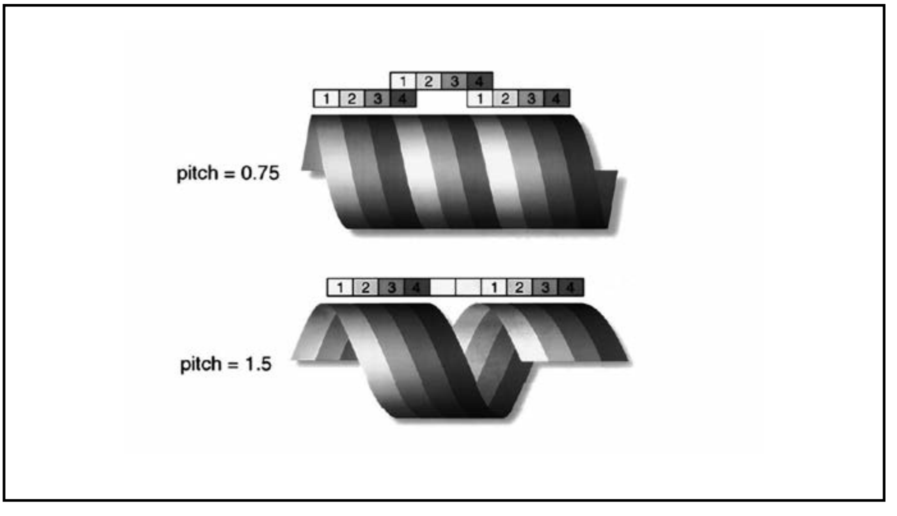

Figure 19.10: A side view of a four-slice scan. In the top diagram the pitch is 0.75. This means that the table travels 3/4 of the beam width (i.e., three channels) in one rotation. This causes detectors 1 and 4 to overlap. When the pitch = 1.5 (bottom diagram), there is an underlap and there is a gap in the coverage. [Reprinted from *The Modern Technology of Radiation Oncology,* vol. 2, J. Van Dyk (ed.), Fig 2.4, p. 38, © 2005; previously adapted and printed in "McCullough, C. H., and F. E. Zink, "Performance evaluation of a multi-slice CT system," *Med Phys* 26:2223–2230, © 1999 with permission from American Association of Physicists in Medicine (AAPM).]

Some radiation therapy departments do not have a dedicated CT unit. There are special considerations when using a diagnostic radiology department CT unit for RT planning. The size of the bore is an important factor. Diagnostic CT scanners generally have a bore diameter of 70 cm. This can be too small for RT for two reasons. The first reason has to do with patient immobilization and positioning devices; the second has to do with the size of the "scanned field of view." The prime example of the first reason is breast treatment where the patient is often lying on a breast board with her arm extended (see Figure 19.11). In this case, the patient may not fit through the bore. It is important that patients be scanned in the same position in which they will receive treatment so that there is no distortion in patient geometry. For accurate treatment planning, patient position must be identical during CT scan and treatment. Immobilization devices such as breast boards, alpha cradles, etc., may not fit through the bore. CT units cannot image over the entire bore aperture. The imaging size is specified by the scanned field of view. This must be large enough to encompass a patient's skin surface completely. The treatment planning system needs complete information about the location of the patient's skin surface to calculate treatment depths accurately. CT scanners with bore sizes up to 90 cm are now on the market for radiation therapy planning purposes.

The couch top of diagnostic CT units is concave. For RT purposes the couch top must be flat like the treatment couch, otherwise patient anatomy will be distorted. Couch inserts are available to make the couch top flat. In fact, a simple board will suffice provided that it is placed level, does not flex, and does not interfere with imaging.

Figure 19.11: A patient undergoing simulation for a breast treatment. The patient is lying on a breast board. Note the position of her arm. This requires a large bore size for CT imaging. (Courtesy of Philips Healthcare, Andover, MA)

For radiation therapy, external lasers are needed for patient positioning and marking. Diagnostic CT units only have internal gantry lasers. The internal lasers show the location of the scan plane. The external lasers are mounted outside the gantry. A set of lateral lasers is mounted either on the floor or on the walls. These project perpendicular lines defining coronal and axial planes, usually 50 cm inferior to the scanning plane (assuming patient goes in head first). An overhead laser projects a sagittal fan beam perpendicular to the scan plane. This laser is sometimes mobile, as it is not possible to move the CT couch laterally.

19.4.2 CT Image Reconstruction

The goal of image reconstruction is to use transmitted x-ray intensity information to determine the μ value for each volume element (called a voxel). The value of μ is then used to construct a gray-scale map, which can be portrayed as an image. The process is described in this and the following section. A simple heuristic explanation follows.

In Figure 19.12 we consider the most elementary "patient" possible, one consisting of a single voxel of known side length x. A single x-ray projection is used. A known intensity, I_0, is incident on the voxel. The transmitted intensity, I, is measured by the detector (see Figure 19.8A). The relationship between the incident intensity and the transmitted intensity is $I = I_0 e^{-\mu x}$ (see chapter 5, section 5.5). In this equation the known quantities are I_0, I, and x. Therefore we can solve for the one unknown μ.

Now let us consider a slightly more realistic example: a patient consisting of two voxels, as shown in Figure 19.13. We again use a single x-ray projection. The relationship between the transmitted intensity and the incident intensity is $I = I_0 e^{-(\mu_1+\mu_2)x}$, where I_0, I, and x are known and μ_1 and μ_2 are unknown. In this case, we have a single equation in two unknowns and we cannot solve for μ_1 and μ_2 without more projections.

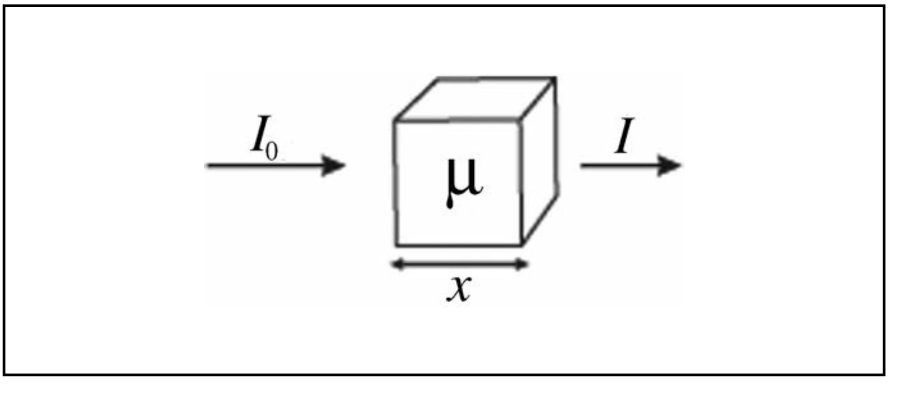

Figure 19.12: A "patient" consisting of a single voxel.

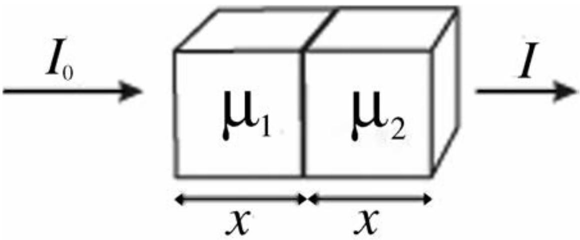

Figure 19.13: A "patient" consisting of two voxels.

Let us now consider a patient consisting of four voxels. We will use four x-ray projections, as shown in Figure 19.14. We have the following relationships between the incident and transmitted intensities:

$$\begin{aligned} I_1 &= I_0 e^{-(\mu_1+\mu_2)x} \\ I_2 &= I_0 e^{-(\mu_3+\mu_4)x} \\ I_3 &= I_0 e^{-(\mu_2+\mu_4)x} \\ I_4 &= I_0 e^{-(\mu_1+\mu_3)x}. \end{aligned} \tag{19.2}$$

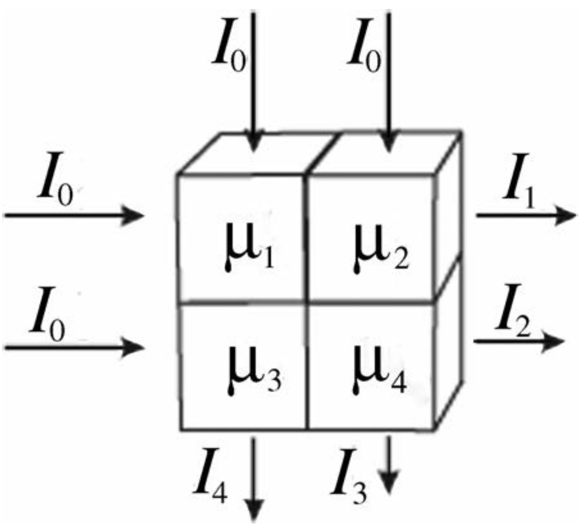

Figure 19.14: A "patient" consisting of four voxels. Four x-ray projections are used.

We have four equations in the four unknowns μ_1, μ_2, μ_3, and μ_4. These equations can be solved for the unknowns.

In general, a patient consists of a large number of voxels *n*. The illustration above has shown that provided there are enough projections, it is possible to solve for $\mu_1, \mu_2, \ldots, \mu_n$; that is, to find the μ value for each voxel. In practice, we are faced with the mathematical task of solving *n* equations in *n* unknowns where the value of *n* may be quite large. Sophisticated methods are used such as: 2-D Fourier transforms or "filtered backprojection." In this way one obtains three-dimensional information about the object imaged. This is called *image reconstruction* (recon). The calculations are carried out on a specialized computer in almost "real time." In the next section we discuss the problem of using the μ values to form an image.

19.4.3 CT Numbers and Hounsfield Units

Each pixel in a CT image requires a numerical gray-scale value for display. The values of μ are converted to CT# or CT pixel value. These are sometimes known as Hounsfield units:

$$\mathrm{CT\#} = 1000\frac{\mu_t - \mu_w}{\mu_w}, \tag{19.3}$$

where μ_t is the linear attenuation coefficient of the tissue in a particular voxel (for a given beam quality) and μ_w is the linear attenuation coefficient for water. Hounsfield units have no dimensions. For air $\mu_t \simeq 0\ \mathrm{cm}^{-1}$ and therefore CT# = −1000 HU. For water $\mu_t = \mu_w$ and therefore CT# = 0 HU. The value of the CT# for dense bone depends on the kVp of the CT. At 100 kVp, $\mu_w = 0.206\ \mathrm{cm}^{-1}$ and $\mu_{\mathrm{bone}} = 0.528\ \mathrm{cm}^{-1}$, therefore CT# = 1000(0.528 − 0.206)/0.206 = +1560 HU. Most CT units have a CT# number range between −1000 HU and +3000 HU. High-density metal clips or prosthetic devices may have CT# approaching +3000 HU.

One HU represents a difference of 0.1% in attenuation coefficient with respect to water. Most CT units have a noise error of ±5 HU. This allows discrimination at the level of ±0.5% in μ_t, enabling good contrast resolution. This sensitivity is what makes CT useful for soft tissue imaging.

CT images are usually 512×512 pixels. CT numbers may span the range from −1000 HU to +3000 HU. There are therefore 4000 possible values associated with each pixel. A 2-byte number associated with each pixel can accommodate this as $2^{16} = 6.6\times10^4$. Storage requirements are therefore 512×512×2 bytes = 0.5 MB for each slice. CT numbers must be converted into a gray level for display. The number of shades of gray that can be perceived by the human eye is at most 256.

One could assign 4000/256 ≈ 16 HU to the same shade of gray, but this would compress the scale and we would lose information. Instead, one should only throw away information that is not needed. This is accomplished by the use of a "window" and "leveling" system. A CT# is chosen that corresponds roughly with the average CT# in the region of interest. This value is called the "level" or center. A "window" width is chosen: for example, 128 shades below the center and 128 shades above the center. Pixels within the window are assigned gray-scale values between 0 and 255. Pixels below the window are set to black and pixels above the window are set to white. The window and level are chosen to obtain the required brightness and contrast for the type of tissue to be examined. Reducing the size of the window increases contrast. Changing the level allows inspection of a different range of CT numbers within the window. As an example of this process, suppose that the level chosen is 200 HU and the window is 500. In this case CT numbers less than $200 - 500/2 = -50$ are displayed as black and CT numbers above $200 + 500/2 = 450$ are displayed as white. One can adjust the window and level to obtain the desired brightness and contrast. This procedure is followed whenever CT images are examined.

For treatment planning with inhomogeneity corrections (see chapter 14, section 14.13), it is necessary to convert Hounsfield units to electron density (electrons/cm^3) by using a calibration curve. These curves are "bilinear" (see Figure 19.15). Calibration curves may be particular to the scanner and the kVp used. They are obtained by scanning a special

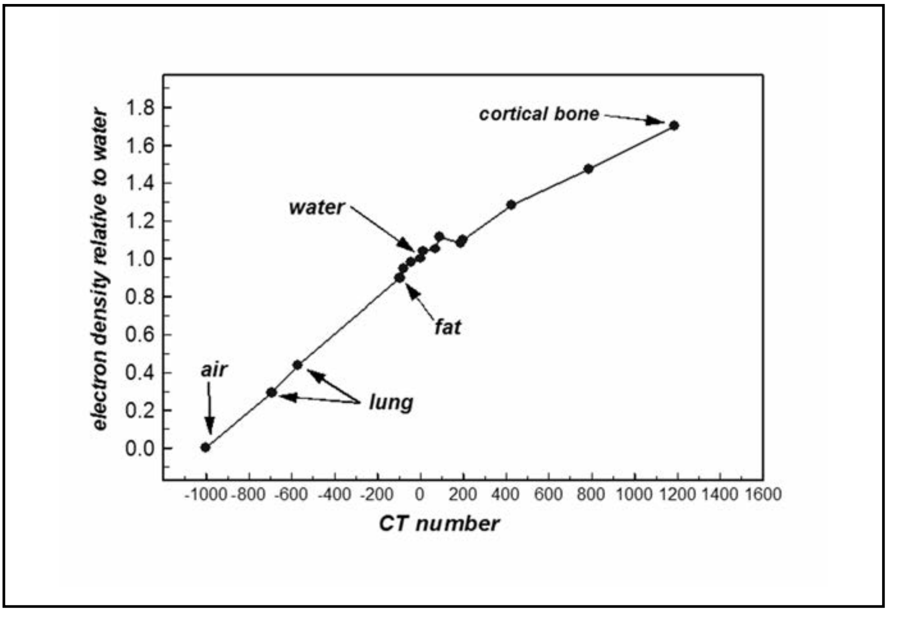

Figure 19.15: The relative electron density as a function of CT# for a representative CT scanner. Some tissues are heterogeneous and it is therefore not possible to assign a single unique CT#. This curve displays a typical bilinear character.

phantom containing about a dozen inserts with various known electron densities. An average CT number is measured for each insert and the electron density can then be plotted versus CT number as in Figure 19.15. The calibration curve is used by the treatment planning system to make inhomogeneity corrections.

High-density materials such as metal prosthetic implants, dental fillings, etc., may lead to streak artifacts. These streaks may have very high CT numbers. These high CT numbers are translated into high electron densities. Such images must be used with care if inhomogeneity corrections are turned "on" in the treatment planning system.

19.4.4 Digitally Reconstructed Radiographs

A plane film radiograph such as produced with a conventional simulator provides a beam's-eye view but not 3-D information. CT provides axial slices but not a beam's-eye view. The data contained in the CT record have information on the linear attenuation coefficient of each voxel. From these data it is possible to mathematically reconstruct a beam's-eye view image for any treatment port. This is known as a *d*igitally *r*econstructed *r*adiograph (*DRR*) because it is constructed from the digital CT data. A DRR is like a simulated radiograph and can be used like an ordinary simulation film for comparison with port films. An example is shown in Figure 19.16. The DRR is constructed by considering ray lines that emanate or diverge from the presumed source (e.g., the target of a linac) and strike an imaging plane a chosen distance away. The

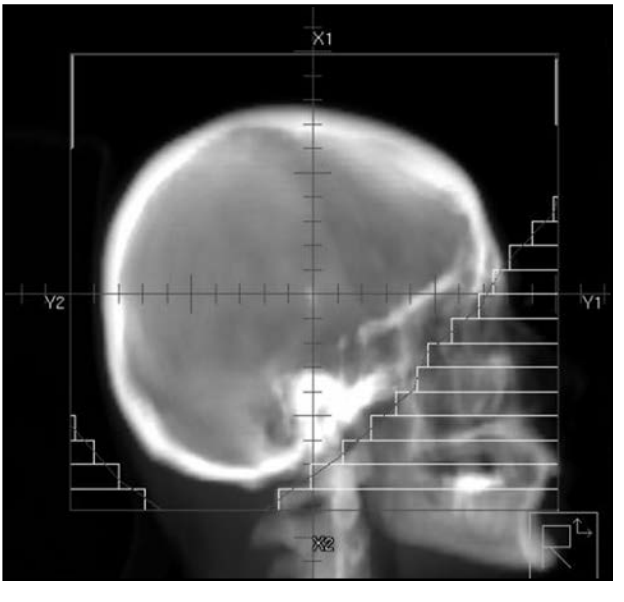

Figure 19.16: A beam's-eye view DRR for a lateral whole-brain irradiation field. The MLC leaf positions for blocking are superimposed.

value of any image pixel is related to the transmission of the associated ray line through the patient. The magnification of a DRR can be specified and various other image parameters can be easily manipulated because of the digital nature of these images. For example, it is possible to emphasize bone. DRR spatial resolution is improved by smaller slice thickness for the CT scan.

19.4.5 Virtual Simulation

The images acquired during a CT examination contain three-dimensional information about the patient's anatomy. These images can be used in conjunction with computer software to perform a virtual patient simulation immediately following CT image acquisition. The virtual simulation software mimics the mechanical motion of the linac. This allows beam's-eye view display for various gantry, collimator, and pedestal angles. The virtual simulation is used to define the treatment isocenter. The patient can then be marked with tattoos before getting off the CT couch. This often involves a set of lateral marks and an anterior or posterior mark. A system is necessary to ensure that the patient is in the same position on the treatment table as during the CT scan. Lasers are used to locate the spot where the skin marks are placed. The simulation software indicates the necessary couch position for laser marking. Radiopaque BBs are sometimes placed over the marks. These will be visible in the CT images and can be used to establish a coordinate system. As CT couches cannot be moved laterally, CT simulators have a moveable overhead sagittal laser. The sagittal fan beam is moved laterally to indicate the correct position of the isocenter on the patient's skin.

19.4.6 4D CT

The term "4D CT" refers to three spatial dimensions plus a time dimension. This is used to track respiratory motion. Let us first consider the effects of motion on CT images.

Refer to Figure 19.17. We imagine a spherical object in a patient's lung. This object is moving up and down sinusoidally with the patient's respiration. This object is shown in the figure (coronal view) at various times throughout two respiratory cycles. These snapshots in time are labeled with numbers 1 through 11. For simplicity we assume pure axial scans (no helical scan). The first axial scan shows the very top of the sphere. A side view of the axial scan slice is shown on the left in Figure 19.17. The top of the sphere is evident in this slice. The table is then indexed for the second axial scan, but by this time the sphere has moved out of the scan plane and does not show up on the axial slice labeled 2. The couch con-

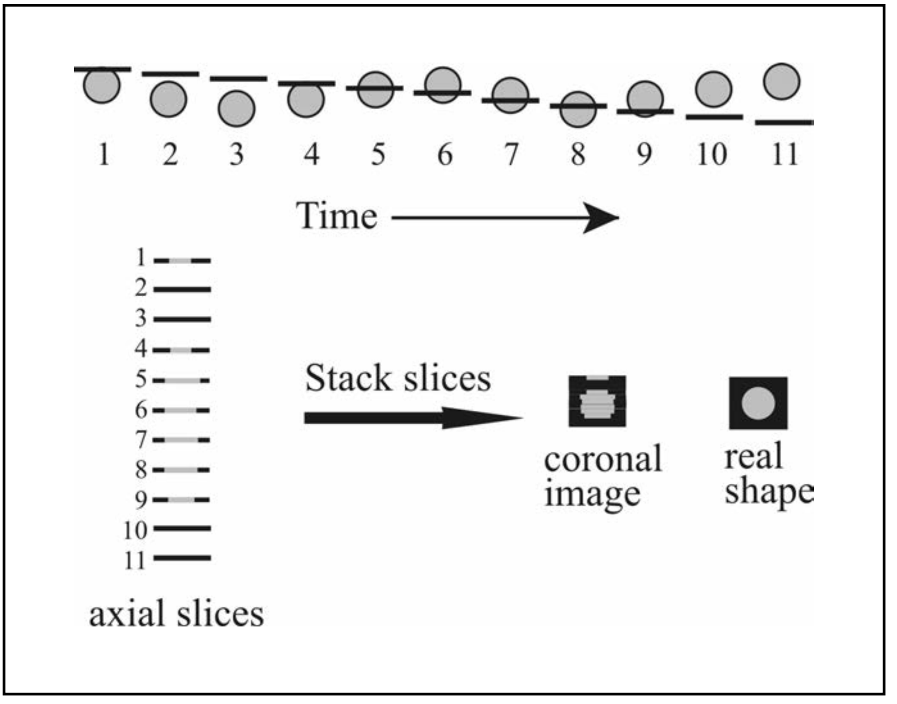

Figure 19.17: Illustration of the effects of motion on CT imaging. The region of interest is a sphere that is oscillating up and down as a result of respiratory motion. See the text for details. (Adapted from *The Modern Technology of Radiation Oncology,* vol. 2, J. Van Dyk (ed.), Fig. 2.5, p. 40, © 2005; previously printed in *International Journal of Radiation Oncology Biology and Physics,* "Can PET provide the 3D extent of tumor motion for individualized internal target volumes?" C. B. Caldwell, K. Mah, M. Skinner, and C. E. Danjoux, vol. 55, pp. 1381–1393, © 2003 with permission from Elsevier.)

tinues to move inward acquiring successive scans. A side view of each axial scan is shown at the bottom left. These can be stacked up to show a coronal image of the object (bottom right). The shape of the image of the object is clearly distorted. Figure 19.18 shows the respiratory motion distortion of a patient's lung tumor.

There are two types of 4-D imaging: prospective gated imaging and retrospective correlation imaging. In both types of imaging a device that monitors respiratory motion is attached to the patient's chest.

Prospective gated imaging is illustrated in Figure 19.19. During axial scans patients hold their breaths at either maximum inspiration or maximum expiration. The patient then resumes breathing while the couch is moved in. The patient then holds his breath again until the next axial scan is completed. The process continues until the entire scan is acquired. A disadvantage of this technique is that it requires patient cooperation and training.

In retrospective correlation (Figure 20) the patient breathes freely during a helical ultra low pitch scan. The pitch is made low

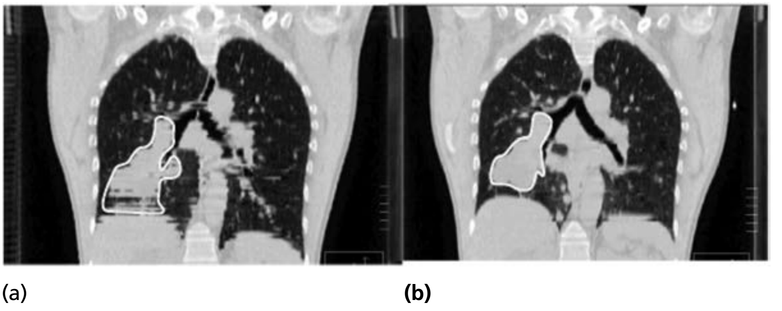

Figure 19.18: (a) A coronal reconstruction of a free breathing spiral CT. The jagged motion artifacts illustrated in Figure 19.17 can be seen in the diaphragm. The outline of a tumor is shown. (b) An expiration-correlated image. The motion artifacts are considerably reduced although not completely eliminated (examine the diaphragm). The shape of the tumor is now significantly different. (Courtesy of Rafael Vaello, TomoTherapy® Inc.)

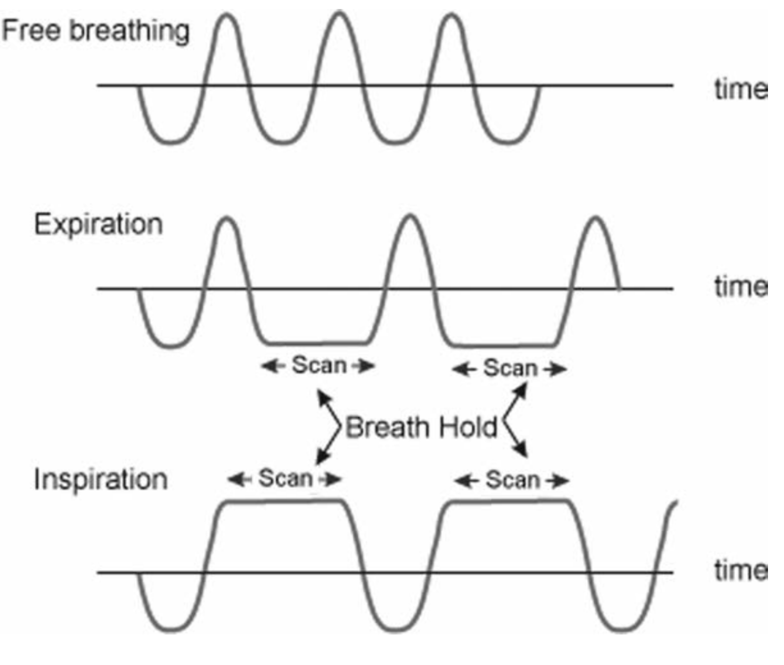

Figure 19.19: Gated prospective 4D CT. The top line shows the patient's free breathing pattern. The middle line shows 4D CT gated on full expiration. The patient is asked to hold his or her breath at full expiration while scanning is underway. This is repeated until the entire volume of interest is scanned. The bottom line shows 4D CT gated on inspiration.

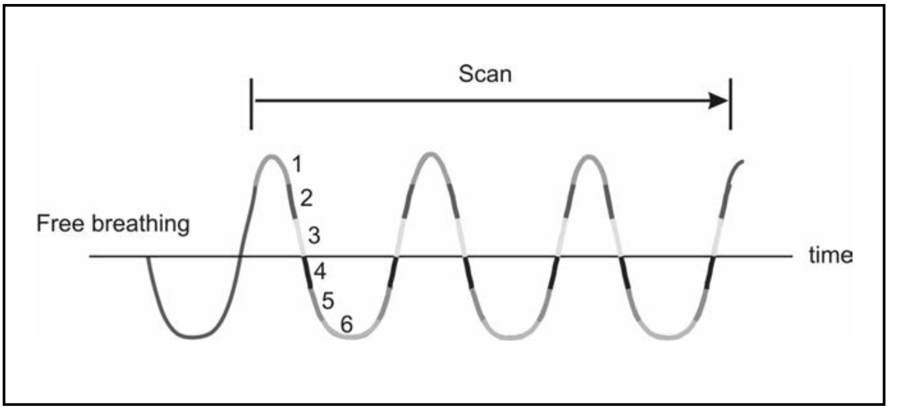

Figure 19.20: Retrospective 4D CT. The patient breathes freely while a very low pitch scan is acquired. Every portion of the relevant anatomy is imaged through a minimum of one respiratory cycle. The breathing cycle is divided into phases. In this figure there are a total of six phases. Eight to ten phases are common. All axial images acquired during a particular phase are grouped together into sets. See COLOR PLATE 14.

enough so that all portions of the anatomy are imaged through several respiratory cycles. The couch should not move more than one detector length in the time it takes to complete one breathing cycle. For a tube rotation time of about 0.5 s and a breathing rate of 12 breaths/min, the pitch should be about 0.1. The respiratory cycle is divided into phases. The operator can choose the number of phases. A typical number is 10. The slices are then arranged in groups according to the phase of the respiratory cycle in which they were acquired. One then has 10 groups of CT scans of the patient's entire chest at 10 moments in time. This can result in over 1000 axial slices. These data can then be used to study the three-dimensional motion of lung tumors in detail. This allows an assessment of the internal target volume (ITV) (see chapter 14, section 14.6).

19.5 Magnetic Resonance Imaging

Magnetic resonance imaging is capable of superb soft-tissue discrimination. MRI is used to diagnose diseases of the central nervous system and musculoskeletal disorders. Breast MRI is used to evaluate lesions discovered with mammography. MRI is widely used as an adjunct to CT in localizing treatment volumes, particularly in the brain. MRI is also capable of direct multi-planar imaging. A CT unit acquires images directly in an axial plane. Images in any other plane, such as the coronal or sagittal, require additional computer processing whereas MR images can be acquired directly in any desired plane. The 2003 Nobel Prize in "Physiology or Medicine" was awarded to Paul Lauterbur and Peter Mansfield "for their discoveries concerning magnetic resonance imaging." This Nobel Prize was somewhat controversial because another important contributor to the development of MRI, Raymond Damadian, was excluded.

An MRI imager appears much the same as a CT imaging unit (Figure 19.7), although the bore is deeper. Some patients experience claustrophobia when in the bore. It may take as long as 10 to 15 minutes to acquire a series of MRI images. A very uniform high-intensity magnetic field is established inside the bore (see chapter 2, section 2.3.6). The field strengths can range from 1 to 3 T and are generally produced with superconducting electromagnets (see chapter 2, section 2.3.4). These magnets require cooling with liquid helium. Higher field strengths allow shorter imaging time and higher signal to noise ratio. MRI units cannot be situated near linear accelerators because the strong magnetic fields would interfere with the motion of the electrons in the linac. Patients with any ferromagnetic implants may not be eligible for an MRI scan. This includes patients with pacemakers or aneurism clips, etc. Exposure to magnetic fields of the strength used for MRI are not known to cause any significant side effects. MRI units are now available with an "open" magnet configuration. These units do not have a donut and thus eliminate claustrophobia.

Nuclear magnetic resonance is based on a fundamentally quantum mechanical effect. A classical physics description of this is simply not possible. We will do our best to explain by drawing classical analogies and "waving our hands." Do not be distressed if you feel that you do not have a detailed or fundamental understanding of this topic. Our task here is to simply provide some flavor of the basic science of MRI. Magnetic resonance imaging is complex and requires years of study to understand fully.

Elementary particles possess an intrinsic angular momentum or "spin." The comic book depiction of this is a small spinning top (like most comic book depictions, this is not reality). A small magnetic field is associated with this spin. The particle acts like a tiny bar magnet (see Figure 19.21) or a "dipole." In an atomic nucleus protons tend to pair up with spins in opposite directions. The same is true for neutrons. When nucleons pair up, their magnetic fields cancel. A nucleus with an odd number of neutrons, protons, or both, however, will have a residual magnetic field. Hydrogen, with a single proton, is one such nucleus. Hydrogen is abundant in tissue and is therefore used for most MR imaging.

In the absence of an externally applied magnetic field, the magnetic fields of the individual nuclei will point in random directions and thus, over the bulk of the material, they will cancel out. If an external magnetic field is applied however, the magnetic nuclei will tend to line up with this field, like iron filings on a piece of paper subjected to a magnetic field. The aligned nuclei will contribute to the external field, reinforcing it. The magnetic field associated with the aligned nuclei is called the "magnetization" and the symbol for this quantity is $\vec{M}$.

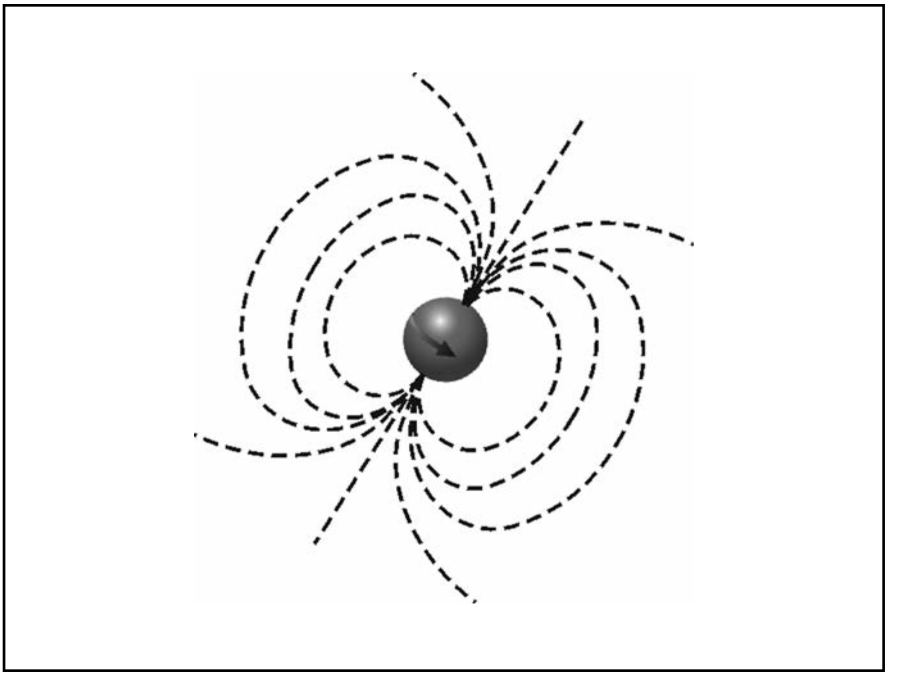

Figure 19.21: Elementary particles such as neutrons and protons possess a property called "spin." A small magnetic field is associated with this. Elementary particles act like small bar magnets.

When the nuclei, which act like little bar magnets, are subjected to an external magnetic field, they behave like a spinning top or a gyroscope in a gravitational field. A top that is spinning will "precess" under the action of gravity (see Figure 19.22). The rotation axis of the top slowly rotates around a vertical axis. In an analogous fashion, nuclei precess in an externally applied magnetic field. The frequency of precession is called the Larmor frequency, ν, and it is directly proportional to the strength of the external magnetic field:

$$\nu = \frac{\gamma B_0}{2\pi}, \tag{19.4}$$

where γ is a quantity that depends on the particular atomic nucleus and is called the gyromagnetic ratio. The value of $\gamma/2\pi$ for protons is 43 MHz/T. For a magnetic field strength of $B_0 = 1.5$ T, the precession frequency is 64 MHz. This is in the radio region of the electromagnetic spectrum just below FM radio in frequency (see chapter 2, section 2.4).

After the external magnetic field is applied to the patient, there are three stages in the process of MR imaging: excitation, relaxation, and detection. *Excitation* involves tipping or rotating the magnetic moment away from the axis defined by $\vec{B}_0$ using the addition of a briefly applied weak

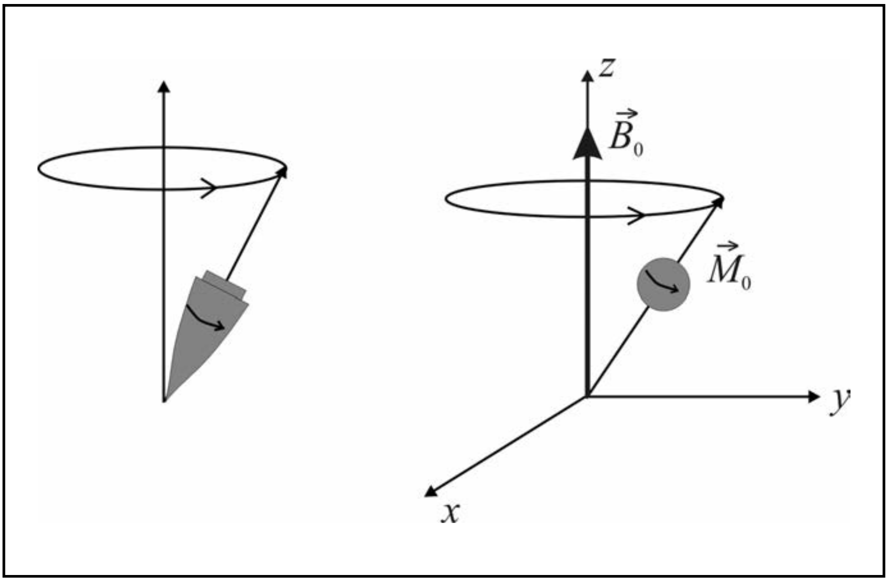

Figure 19.22: A spinning top precesses in a gravitational field; that is, the spin axis itself rotates around a vertical axis. In a similar way, the magnetic moment of a proton precesses around the direction of an externally applied magnetic field. The direction of the magnetic field is taken to be along the z-axis.

magnetic field in the form of a radio frequency (RF) pulse. The angle through which $\vec{M}$ is tipped can range from 0° through 180°, depending on the duration of the pulse. If $\vec{M}$ is tipped 90°, this is called a 90° pulse. After the RF pulse, $\vec{M}$ "wants" to return to its undisturbed direction along $\vec{B}_0$. This is *relaxation.*

After excitation, the amplitude of the component of $\vec{M}$ in the x-y plane will decrease at a rate 1/T2 and the z-component will increase at a rate of 1/T1. The values T1 and T2 depend on the external field strength B_0 and on the characteristics of different types of tissue. As the nuclei return to their equilibrium state, they emit an RF signal which can be detected by an RF coil. This is *detection.* The closer the receiving coil to the patient, the better. A number of different types of RF coils are available: head coils, body coils, and coils for other body parts.

The precession frequency depends on the applied magnetic field [see equation (19.4)]. If small gradients are deliberately introduced into this field, then the precession frequency will vary with position in the patient. In this way spatial information can be encoded in the data and this information can be used to reconstruct an image.

Typical images are one of three types: proton density or spin density, T1 weighted, or T2 weighted (see Figure 19.23). These are produced using different combinations of echo time (TE) and repetition time (TR). T2 weighted images have TE of 60 to 100 ms and TR of about 3000 ms. T1 weighted images have TE about 10 ms and a value of TR comparable to T1 for the tissue of interest (about 500 ms at

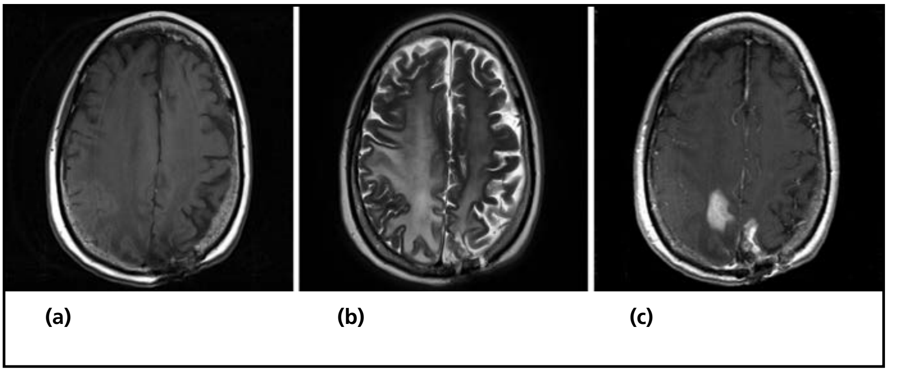

Figure 19.23: Three axial MRI images of a GBM tumor. (a) is a T1 weighted image. This image displays the tumor and edema as dark. (b) is T2 weighted. This image displays the tumor and edema as light. T2 images do not show fat and they highlight CSF and gray matter. The image in (c) was made with a gadolinium contrast agent. (Courtesy of Brigham and Women's Hospital, Boston, MA)

1.5 tesla).[4] Fluid attenuated inversion recovery (FLAIR) is a pulse sequence that creates images that have T2 weighted contrast for brain tissue but in which signals for CSF are suppressed.

FLASH stands for fast low angle shot, and about 70% of MRI is done this way. A contrast agent that is commonly used contains the paramagnetic element gadolinium.

MR images by themselves are generally not adequate for treatment planning purposes. They are more susceptible to spatial distortions than CT. It is important to have reliable geometric information about the patient. The determination of the location of a voxel in MRI is governed by the magnetic field gradients. Any irregularities in the magnetic field can therefore cause spatial distortion. In addition, MR imaging takes longer than CT and therefore there is an increased likelihood of distortion due to patient motion. Furthermore, MRI does not provide information about electron density, which is necessary for inhomogeneity corrections in dose calculations. The physical dimensions of the scanner and its accessories limit the use of immobilization devices. Dense bone contains very little hydrogen and therefore the bone signal is weak. For this reason useful DRRs cannot be generated for comparison with portal images. Instead of being used by themselves, MRI images are often used in conjunction with CT data for treatment planning. This requires image fusion, which is discussed in the next section.

[4] "MRI in Radiation Treatment Planning" by Y. Cao and L. Chen, pp. 401–424 in *Integrating New Technologies into the Clinic: Monte Carlo and Image-Guided Radiation Therapy,* AAPM 2006 Summer School Proceedings, AAPM Medical Physics Monograph No. 32, B. H. Curran, J. M. Balter, and I. J. Chetty, Program Directors, 2006.

19.6 Image Fusion/Registration

For the purpose of treatment planning it is very useful to be able to combine or correlate images from different modalities, in particular CT and MRI. Tumors frequently appear very different on MR images than on CT (if they show up at all). Image fusion (or registration, as it is sometimes called) is the process of placing two sets of images on the same coordinate system so that they can be superimposed like an overlay or viewed simultaneously. This correlation combines the advantages of CT with another modality such as MRI or PET. Most treatment planning systems offer the option of image fusion. Sometimes it is desired to register two sets of CT images obtained on different dates. The process of image-guided radiation therapy (IGRT; see section 19.10) depends on image registration.

We first consider the problem of registration for images of an object that is a rigid body. A rigid body is one that cannot change shape or be deformed. The two objects in the different image sets can be brought into coincidence by coordinate translations (shifts) and rotations. It is best if both sets of images are obtained at about the same time, ideally the same day. The patient should be in the same position for each imaging modality. Ideally any immobilization devices should be used for both sets of scans. We will discuss three methods for registration of a rigid body: point-to-point matching, surface to surface matching and voxel-to-voxel matching.[5]

In point-to-point matching, a set of corresponding reference points or fiducial markers is necessary in both sets of images. These can be externally placed markers positioned in key locations on the patient's skin. Adhesive markers are available commercially, which show up clearly in both CT and MRI images. A bare minimum of three points in each image, not all lying in the same plane, is required and more are preferred. Once the fiducial points are specified, the image fusion software shifts (translates) and rotates the images so that they correspond to one another. In the absence of externally placed markers, which are preferable, internal anatomical reference points may be used. It may not be easy to find anatomical points of reference that can be clearly seen in both image sets.

Anatomical surfaces may be easier to delineate in both image sets than discrete points. Surface matching involves matching anatomical surfaces in the two images. Voxel-to-voxel matching uses all of the information in the images. In this technique there is an attempt to correlate all of the voxels to one another. One shortcoming of this technique is that parts of the image may be unreliable. An example is the mandible, which may be in different positions with respect to the skull

[5] *Radiation Oncology: A Physicist's Eye View* by M. Goitein, 2008, p. 48.

in the two image sets. A method of image registration that has achieved some success involves the maximization of "mutual information."[6] Although the pixel intensities of tissues may differ in different modalities, there is a relationship between them. For example, bone is bright in CT images and dark in MRI images. Mutual information registration relies on the predictable relationship between corresponding tissue types in the two image sets.

If there are significant differences in the shape of the patient between the two image sets, then deformable image registration is desirable. Differences in shape may result from imaging on different days, in different positions, or with and without immobilization devices. Respiratory motion may cause deformation also. Deformable image registration is not yet commonly available in commercial treatment planning software.

For treatment planning, the primary set of images is the CT set. Dose calculations are done from this set. Once the software has performed the fusion, it is up to the user to examine the images to assess the quality of the result (see Figure 19.24). Do not take the quality of the fusion for granted. The correlation of the two image sets must be carefully examined. The radiation oncologist can draw tumor outlines (GTV, CTV, etc.) on the fused MR (or PET) images, which will then automatically be transferred to the CT images used for dose calculations. The reliability of this process depends critically on the quality of the registration.

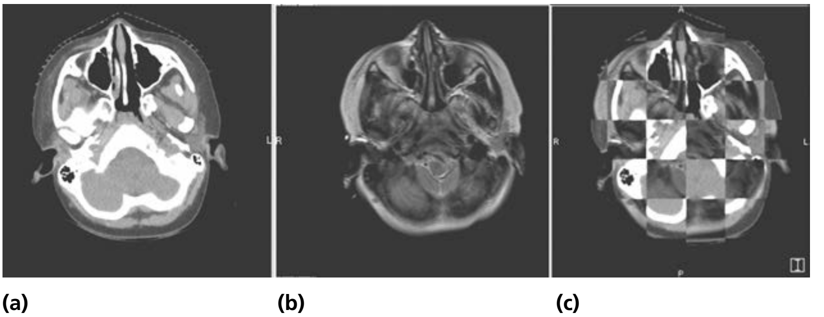

(a) (b) (c)

Figure 19.24: An example of image fusion between CT and MRI images. The image in (a) is the CT image. The image in (b) is the reconstructed (fused) MRI image that corresponds to this. The quality of the fusion (which is marginal) is assessed from the "checkerboard" image in (c). Alternating squares are either CT or MRI.

[6] Chen et al., in Chapter 2, Imaging in Radiotherapy in *Treatment Planning in Radiation Oncology,* 2nd edition (F. Khan, ed.).

19.7 Ultrasound Imaging

The use of ultrasound for diagnostic imaging is widespread in medicine. Ultrasound is one of the three means of imaging soft tissue. Ultrasound equipment is relatively inexpensive and there is no ionizing radiation exposure. An ultrasound system is shown in Figure 19.25. Ultrasound is frequently used as an adjunct to mammography for breast cancer detection. In radiation therapy ultrasound is used for treatment planning, particularly for prostate brachytherapy implants, and for treatment position verification, primarily for external beam prostate therapy (see section 19.10).

Sound waves are longitudinal waves—a small parcel of matter in the medium oscillates back and forth in the direction in which the wave moves (see Figure 19.26). This contrasts with transverse waves in which the motion of the medium is perpendicular to the direction of wave travel (as in Figure 2.12). Examples of transverse waves are waves on a string or (approximately) waves on the surface of water.

Figure 19.25: Ultrasound imaging cart. (Courtesy of Siemens Medical Solutions USA Inc., Concord, CA)

Sound can be thought of as a compressional wave. This is illustrated in Figure 19.26. This figure shows a snapshot at an instant in time of a compressional wave.

The speed of sound in a given medium depends on the elastic properties of that medium. The speed of sound in soft tissue is approximately 1540 m/s. Ultrasound imaging is dependent on differences in the sound speed of various tissues. When an ultrasound wave is incident upon an interface where the sound velocity changes, part of the wave will be reflected. It is these reflections that form the basis for conventional ultrasound imaging.

The frequencies of audible sound waves extend from about 20 Hz up through perhaps 20 kHz (if you are a child with excellent hearing). Ultrasound frequencies are approximately 5 MHz, well beyond the range of human hearing (hence the name ultrasound). As an example, we will calculate the wavelength of a 3.5 MHz sound wave in soft tissue. We use the equation $\nu\,\lambda = c_s$ [essentially equation (2.19)] where c_s is the sound speed: $\lambda = c_s/\nu = (1540\ \text{m s}^{-1})/(3.5\times10^{6}\ \text{s}^{-1}) = 4.4\times10^{-4}$ m or 0.44 mm. To achieve high spatial resolution, small wavelength is desirable. If the wavelength is comparable to, or larger than, the object to be imaged, then the wave will simply "bend" (diffract) around the object and no clear (specular) reflection will occur. It is apparent from the previous calculation that high frequencies are necessary to achieve small wavelength, and this is why ordinary audible sound would be inadequate for high-resolution imaging.

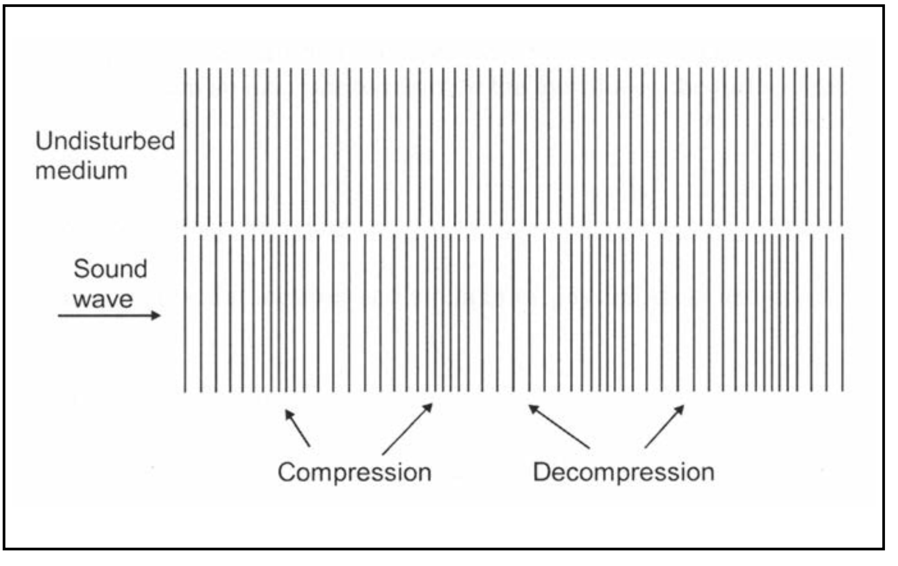

Figure 19.26: A longitudinal sound wave. The top portion of the figure shows an undisturbed medium (no sound wave). The bottom portion is a snapshot at a particular instant in time showing regions of compression and decompression. A small element in the medium moves back and forth horizontally as the wave passes by from left to right.

Ultrasound waves are produced and detected by a device called a transducer. A transducer is any device that converts one form of energy to another. The ultrasound transducer converts electrical energy to mechanical energy. An electrical signal fed into the transducer converts electrical energy to mechanical vibrational energy. The transducer is coupled to the patient surface (sometimes a coupling gel is used to get good mechanical contact) and sound is transmitted into the patient's body. A transducer also detects and converts the reflected sound waves into electrical energy—similar in function to a microphone. The reflected wave provides the basis for image formation. The longer it takes a wave reflected from an interface to return to the transducer, the further the interface is from the transducer.

19.8 Functional/Metabolic Imaging

Functional imaging shows the location and strength of physiological activity at the cellular and molecular levels.

The promise of functional imaging:

(1) *Improve disease detection:* functional imaging is capable of detecting microscopic disease.
(2) *Cancer staging:* functional imaging may reveal areas of disease not visible with anatomical imaging. For example, it may more readily reveal the existence of metastatic disease.
(3) *Treatment planning:* functional imaging may be of assistance in planning radiation therapy by providing more accurate localization of disease; radioresistance of tumor, tumor phenotype; identify areas of hypoxia that may require a higher dose. In the future it may become possible to identify a biological target rather than simply an anatomical target.
(4) *Response to therapy:* may allow a more rapid indication of cellular response to therapy.
(5) *Earlier detection of recurrence.*

Positron emission tomography (PET) provides metabolic information such as glucose metabolism rates. Cancer cells generally metabolize glucose at higher rates than normal cells. The patient is administered a pharmaceutical tagged with a positron emitter either by injection or inhalation. PET scans frequently employ F-18 (fluorodeoxyglucose, ^{18}F-FDG). This is a marker for glucose metabolism. The distribution of activity throughout the patient is imaged. FDG uptake is enhanced in most malignant tissues and in some benign structures as well. FDG uptake can be used to measure tumor response to treatment as well as for initial staging. New PET radiopharmaceuticals that are more specific markers of tumor activity are under development.

F-18 undergoes positron decay with a half-life of 110 minutes. The positron emitters used in PET imaging have a short lifetime and therefore the supply for these isotopes must be physically close at hand. Positron emitters are produced in cyclotrons. Therefore PET facilities must either have a cyclotron on site or a cyclotron must be located relatively nearby.

There is a waiting period of about an hour between injection of FDG and the scan to allow time for uptake. PET scan data acquisition takes on the order of 20 minutes. This is clearly a problem when significant respiratory motion is present. 4D PET scanning is on the horizon and is expected to be available soon.

The positrons travel only a short distance before annihilating and forming two 0.5 MeV photons that travel in almost completely opposite (180°) directions. These photons are detected by scintillation detectors made of bismuth germanate (BGO) or (LSO:ce).[7] The visible photons that emerge from the scintillator are detected by photomultiplier tubes.

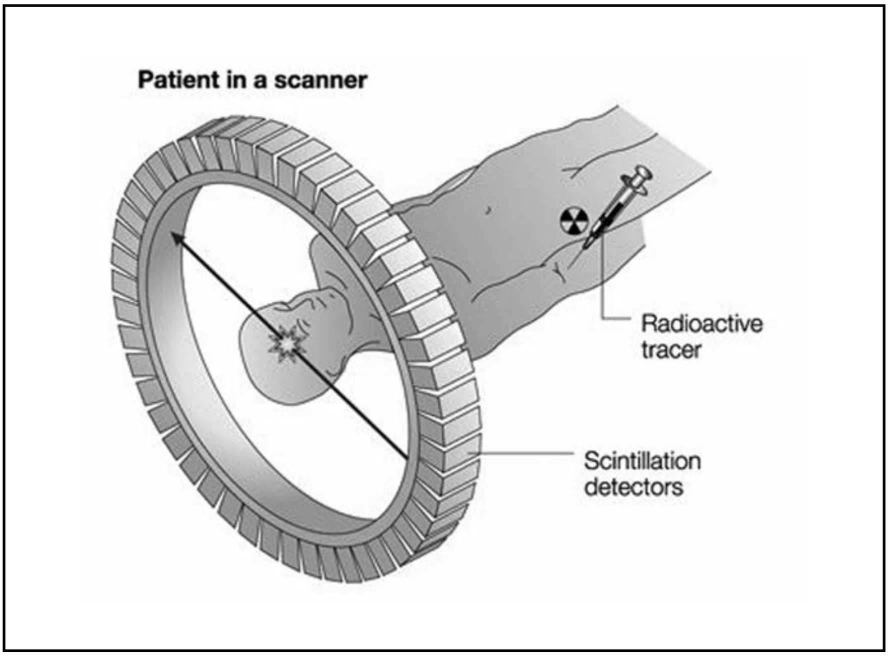

Figure 19.27: The detectors in a PET scanner form an axial ring around the patient. Event counting is based on annihilation coincidence. Events must occur nearly simultaneously in opposite detectors or they are rejected. Coincidence detection confirms that the annihilation must have occurred somewhere along the line joining the detectors. (Reprinted by permission from MacMillan Publishers Ltd: *Nature Reviews Cancer,* vol 4, pp. 457–469, "The potential of positron-emission tomography to study anticancer-drug resistance," C. M. L. West, T. Jones, and P. Price, © 2004.)

[7] Sasa Mutic in "Use of Imaging Systems for Patient Modeling PET and SPECT" by S. Mutic, pp. 375–400, in *Integrating New Technologies into the Clinic: Monte Carlo and Image-Guided Radiation Therapy,* AAPM 2006 Summer School Proceedings, AAPM Medical Physics Monograph No. 32, B. H. Curran, J. M. Balter, and I. J. Chetty, Program Directors, 2006.

PET uses annihilation coincidence detection to reconstruct axial images showing the activity distribution or uptake. There is a series of detectors in a ring around the gantry bore (see Figure 19.27). Each detector in the ring is paired with detectors on the opposing side of the ring. If a signal is detected in one of the detectors, a gating circuit "listens" for a signal in the paired detectors on the opposite side for a short interval of time called the coincidence window. If a signal is detected during this interval, it is assumed that the signal must represent a true annihilation photon corresponding to the detection on the opposite side. It is then known that the annihilation must have occurred somewhere along the line joining the two detectors. If no second signal is detected during the coincidence window, the original signal is discarded. The coincidence window is usually about 5 to 10 ns in duration, which corresponds roughly to a time $t = D/c$, where D is the maximum thickness of the patient and c is the speed of light.

Currently, 90% of PET scans are for oncology purposes. Combined PET/CT scanners now completely dominate the market. In a PET/CT unit the two gantries are combined in the same housing (see Figure 19.28). PET/CT machines have the advantage that fusion is more accurate because the patient is scanned on the same couch and almost at the same time as the CT scan. Therefore the patient is positioned identically in the two scans. Fusion of separate PET images and CT is more difficult because of the low spatial resolution of PET images (on the order

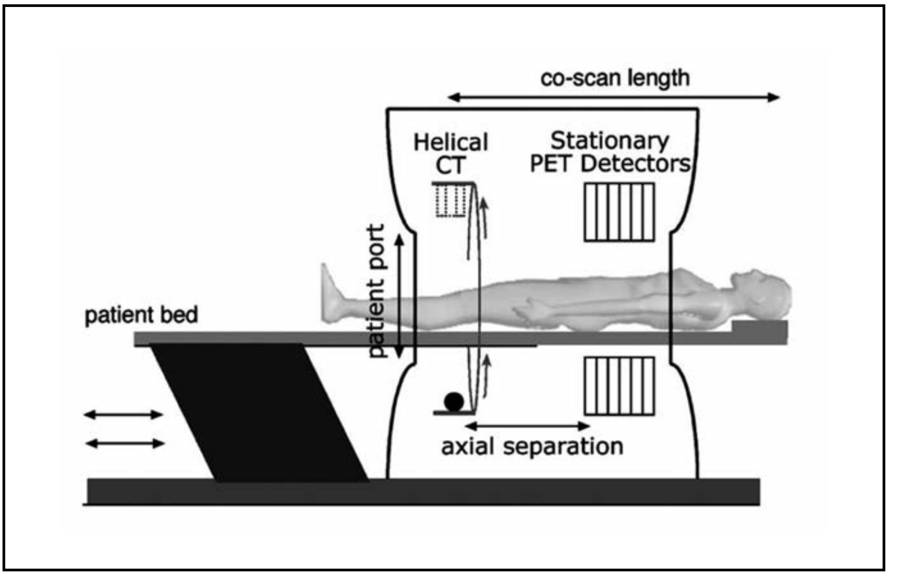

Figure 19.28: A PET/CT unit. This is a long bore design in which the housing covers both the PET and CT unit. (Reprinted from *The Modern Technology of Radiation Oncology,* vol. 2, J. Van Dyk (ed.), Fig. 2.14, p. 63, © 2005; previously printed in *Radiologic Clinics of North America,* vol. 42, issue 6, A. M. Alessio, P. E. Kinahan, P. M. Cheng, H. Vesselle, and J. S. Karp, "PET/CT scanner instrumentation, challenges, and solutions," pp. 1017–1032, © 2004 with permission from Elsevier.)

of 5 mm). The CT data allow for attenuation corrections of the PET image, resulting in sharper images and significantly shorter (by up to 40%) PET scan time.[7]

The uptake of FDG can be quantified by the use of the standard uptake value (SUV), which is defined as:

$$\mathrm{SUV} = \frac{\text{Activity per unit volume / decay factor}}{\text{Injected activity / body mass}}, \qquad (19.5)$$

where the activity per unit volume is measured in units of MBq/ml, the decay factor is the fraction of decay between administration and the time of the scan, and the injected activity/body mass is in units of MBq/g. The SUV will vary throughout a tissue. The maximum SUV is a more useful parameter than average SUV.[8] SUV may not be useful in tissue that normally has a high SUV such as the brain (high glucose metabolism rate) and the kidneys (the kidneys clear FDG from the body). It is common to use an SUV threshold of 2.5 as an indicator of the presence of malignant tissue although SUV values have not been shown to be useful for defining GTV boundaries.[9]

19.9 Portal Imaging

How do we verify correct treatment delivery?

(1) *Positional accuracy:* Are we hitting the target?
Portal imaging.

(2) *Dosimetric accuracy:* Are we delivering the right amount of dose to the target?
In vivo dosimetry: TLDs, diodes, MOSFETs, etc., discussed in chapter 8 (see also chapter 18, section 18.3.4). In the future these two may be "married" with portal imagers that can simultaneously image and verify dose.

Portal images can be acquired with either film (rapidly disappearing) or electronic portal imaging devices (EPIDs). Portal images are used to verify both the shape of the aperture and the position of the central axis with respect to the patient's anatomy. It is common to superimpose an open field on the portal aperture field so that surrounding anatomy can be viewed for reference. This is sometimes referred to as a "double exposure."

---

[8] The SUV must be used with caution. Caldwell and Mah have pointed out that some researchers refer to SUV as standing for "silly, useless, value."

[9] C. B. Caldwell and K. Mah in chapter 2, *Imaging for Radiation Therapy Planning, The Modern Technology of Radiation Oncology,* Volume 2, J. Van Dyk (ed.), page 67.

19.9.1 Port Films

(1) *Localization film:* Exposure is short compared to the daily treatment time, need sensitive film.
(2) *Verification film:* Exposure is for the duration of the treatment delivery with that field, use slow film such as Kodak XV film.

These films are compared with films from the simulator or DRRs produced by the treatment planning system. The purpose is to verify targeting.

Why is portal image quality so poor compared to diagnostic images?

(1) *Poor contrast:* Predominant interaction is Compton, weak dependence on Z, very little differential absorption is seen compared to diagnostic films.
(2) *Scattered photons and secondary electrons:* Scattered photons are not easily removed, cannot use a grid.
(3) *Large penumbra:* Geometric + phantom scatter.

The quality of port images degrades with increasing beam energy and patient thickness (>20 cm). Portal images should be made using the lowest energy photon beam available.

For portal films, the film is placed in a special cassette. Compton recoil electrons form the image on the film, not the photons directly. The secondary electrons generated in the patient, treatment couch, etc., tend to smear out images because electrons are very easily deflected. We want to filter out these electrons. We would also like to have some build-up in front of the film. For these two reasons metal screens are used inside portal film cassettes. The screen is placed in close contact with the film. The screen is made of a high-density material such as lead or copper. It is common to use a copper screen about 1 mm thick. Port films are not made in real-time—they have to be developed. They are impractical to do before every treatment. This leads to a motivation to have real-time imaging.

19.9.2 Electronic Portal Imaging Devices[10]

There are three major types of electronic portal imaging devices (EPIDs):

(1) Screen camera systems.
(2) Matrix ion chamber.
(3) Flat-panel arrays.

This field is evolving rapidly. Linac manufacturers have now moved to flat-panel arrays.

[10] Much of the information in this section is taken from *The Modern Technology of Radiation Oncology*, J. Van Dyk (ed.), 1999.

Screen camera systems use a video camera and a mirror oriented at a 45° angle. A phosphor-coated metal plate produces visible light photons, which are imaged by the camera. Camera images are digitized at 30 frames/s, then averaged to produce a final image. They have good resolution, but they are bulky and tend to get in the way.

Matrix ion chamber EPIDs consist of an array of ionization chambers. One design uses a 256×256 array of ion chambers with an electrode separation of 0.8 mm and is filled with a volatile liquid. When the liquid is irradiated, ion pairs are formed which are collected when a bias is applied between the electrodes.

Flat-panel arrays have replaced camera-based and matrix ion chamber EPIDs. The image quality is superior to the older technology. The flat-panel arrays overcome the bulkiness of camera systems and the relatively long irradiation times for matrix ion chamber EPIDs. Flat-panel EPIDs are solid-state devices in which amorphous silicon (a-Si) is deposited on a thin substrate, usually 1 mm of glass. Amorphous silicon is highly resistant to radiation damage and can therefore be placed in the direct beam. Each pixel is a photodiode, which detects light generated by a screen/phosphor combination. The screen/phosphor combination consists of a metal plate and a phosphor screen. The metal plate removes secondary electrons generated in the patient as well as low-energy scattered photons. A commercial model is the Varian aS500 Portal Vision with an array size of 40×30 cm^2 and 512×384 pixels (see Figure 19.29). This model has a 1 mm copper plate and a gadolinium oxysulfide (Gd_2O_2S) screen. Each pixel value is represented by a 16-bit word.

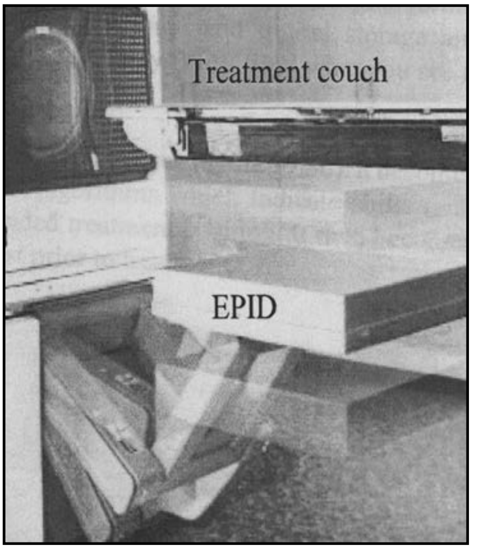

Figure 19.29: A portal imager on a robotic arm. The imager folds away at the base of the gantry when not in use. The arm can move the imager vertically and horizontally. (Courtesy of Varian Medical Systems, Inc. Copyright © 2010. All rights reserved.)

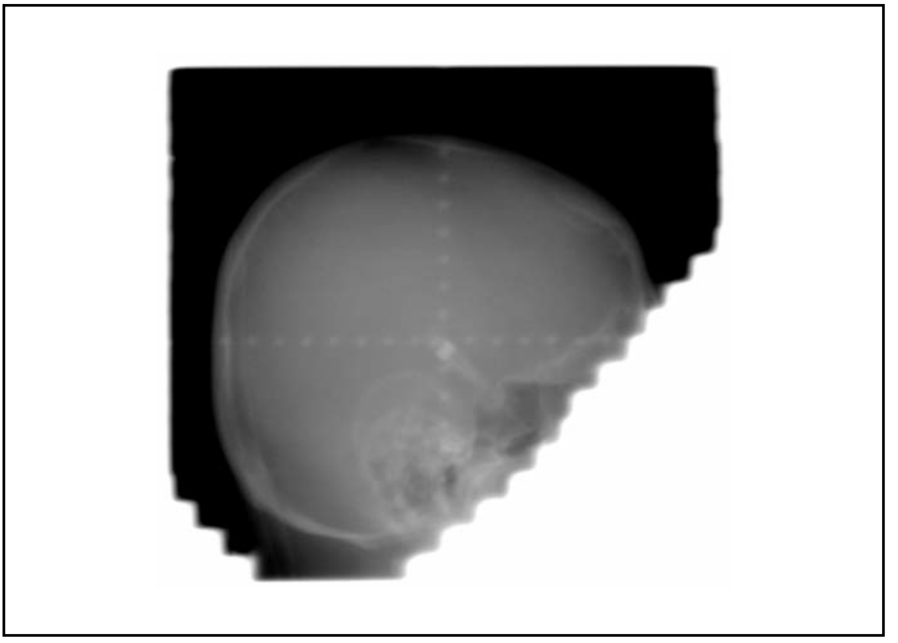

Figure 19.30: An electronic portal image made with a flat-panel array. This is a lateral skull image made with a 6 MV beam using 2 MU for a whole-brain irradiation field. The graticule is visible in the image. The faint outline of a diode placed on the patient's skin is visible at the center. Compare this image with the DRR for the same patient in Figure 19.16.

What are the differences between the use of EPIDs and film? One obvious difference is an immediate result without having to wait for processing. EPIDs are sensitive to the dose rate whereas film is sensitive to the total cumulative dose. For the EPID, one sets a specific number of MU regardless of the patient thickness. For film one must take into account the patient thickness. The digital format of EPID images allows image enhancement, window and leveling, and digital storage and dissemination. Both film and EPID images are available in hard copy. With film, what you see is what you are stuck with.

The ease of use of EPIDs makes more frequent imaging easily feasible (see Figure 19.30). It becomes feasible to image the patient daily and to use correction algorithms that indicate shifts (and possibly rotations) of the patient with respect to the intended treatment position. It then becomes possible to move the patient into the intended position just prior to treatment.

19.10 Image-Guided Radiation Therapy

Image-guided radiation therapy (IGRT) employs imaging of soft tissue or implanted markers to ensure target positioning prior to treatment. The location of key anatomical structures or markers is compared to the expected location (based on CT images used for treatment planning) and the patient is moved if necessary. The geometric accuracy of treatment delivery is limited by three factors: set up uncertainty, intrafraction target movement, and interfraction target movement. These issues have been discussed in chapter 14, section 14.6. The desire for highly conformal therapy is the motivation for IGRT. IGRT reduces the chance of a geometrical miss and allows a reduction in the size of the PTV with all the benefits that follow: fewer treatment complications and/or dose escalation.

There are quite a variety of commercially available systems for IGRT. Conventional linear accelerators can now be purchased with optional on-board kV imagers that are capable of cone beam CT (see Figures 19.31 and 19.32). The imager consists of an x-ray tube and a flat-panel detector. The axis of the x-ray beam is perpendicular to the MV beam axis. These are now widely available. Another option is a conventional linac and a CT scanner that share a common couch. A third option is CT images generated from the same MV beam that is used to treat the patient. This technique is used on an innovative treatment machine that delivers "tomotherapy." We defer a discussion of tomotherapy units to the next chapter. Ultrasound is used in some clinics to image the prostate prior to prostate radiotherapy. Yet another choice is implantable markers that are available from several vendors. These

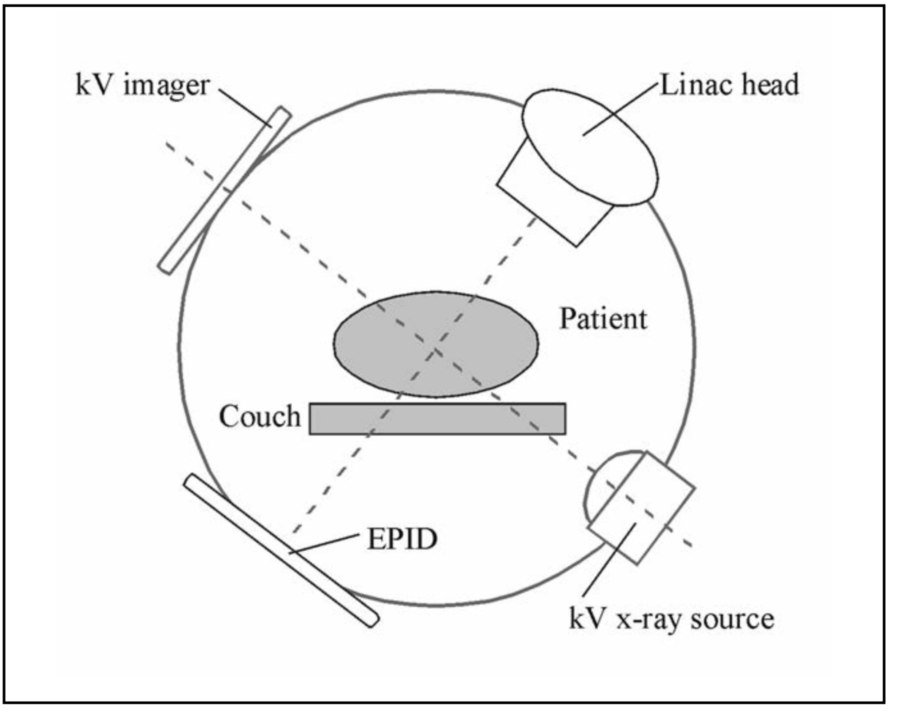

Figure 19.31: A conventional linac with on-board kV cone beam imaging. The gantry rotates around the patient with the MV beam off and the kV beam on. Given a sufficient number of projections, a set of axial CT images may be reconstructed.

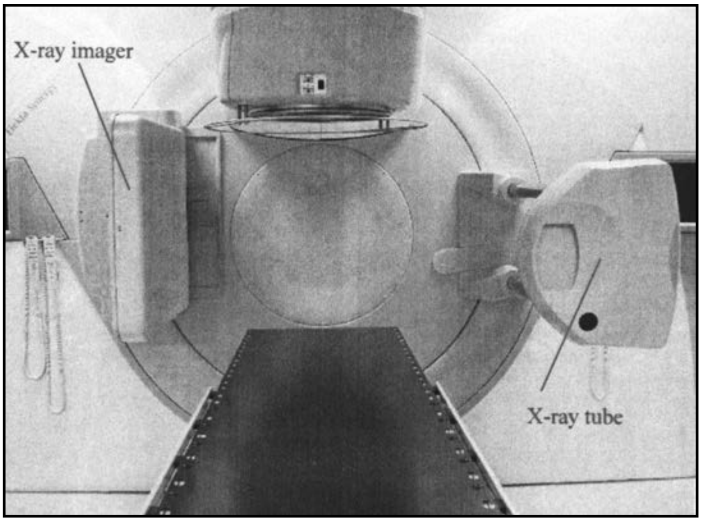

Figure 19.32: The Elekta Synergy® with on board kV imager. (Courtesy of Elekta, Norcross, GA)

markers can be observed in MV images. Provided that there are a sufficient number of these, the location and orientation of the organ in which they are embedded can be determined. Markers have been used widely for prostate treatments. A more exotic illustration of IGRT is provided by the imaging capabilities of a robotic linac (see the discussion of radiosurgery in chapter 20).

For kV cone beam CT the gantry rotates around the patient while the kV x-ray tube is on and the MV beam is off. During gantry rotation the kV imaging panel is acquiring numerous projections. The projection data can be reconstructed to provide a set of CT axial images. The shape of the kV x-ray beam is a cone and thus this modality is referred to as cone beam CT (CBCT). For IGRT purposes it is crucial that the MV beam and the kV beam share the same isocenter. During gantry rotation the x-ray tube and imager may sag or flex. It is necessary to correct for this by use of a "flexmap" which characterizes the flex with gantry angle.

CBCT images can be compared to the treatment planning CT. The CBCT software on the linac allows the operator to determine the shift in patient position that will best bring the two sets of images into alignment (see Figure 19.33). In general, this requires three shifts (translations), one in each of three perpendicular coordinate directions and rotations about three axes. Rotational correction is available on some specialized linacs. Linacs without this capability use the three translations that give the best fit. If the movements are small, the table can be moved automatically from the control console without having to enter the treatment room.

Ultrasound is used in some clinics to image a patient's prostate gland prior to delivery of radiation for prostate cancer (see Figure 19.34).

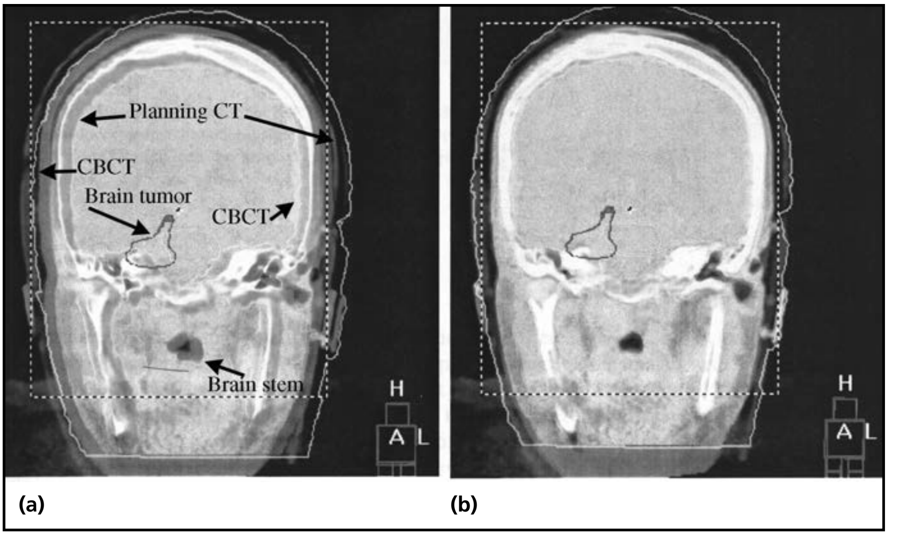

Figure 19.33: Cone-beam image-guided radiation therapy. (a) A patient's cranium as imaged with the Elekta XVI (x-ray volume imaging) system shown in Figure 19.32. Contours of a brain tumor (in red) have been imported from the treatment planning CT. This is the view prior to image registration. The planning CT image is in pink and the cone beam CT is in green. There is a clear mismatch between the two sets. (b) This is the same as (a) except that this is the image after registration. The patient is now positioned very accurately for treatment. (Courtesy of Elekta, Norcross, GA) See COLOR PLATE 15.

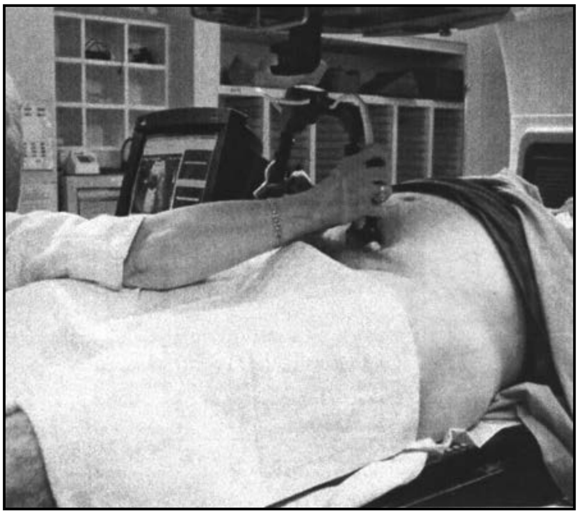

Figure 19.34: Prostate ultrasound localization for IGRT. A therapist is holding the transducer against the patient's skin. The head of the linac and the docking station can be seen at the top of the photo. (Courtesy of Best Medical, Springfield, VA, www.TeamBest.com)

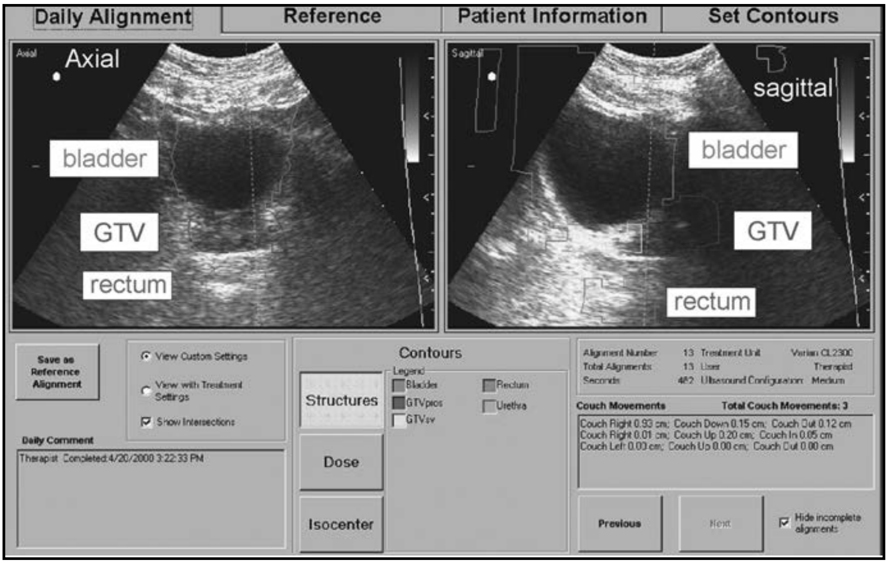

Figure 19.35: A screen capture from the NOMOS BAT (B-mode Acquisition and Targeting) ultrasound IGRT system. The image on the left is an axial image. A sagittal image is shown on the right. The operator has superimposed contours of the bladder, GTV, and rectum from the treatment plan. These contours have been aligned with the corresponding structures in the ultrasound images. The shift necessary to bring about this alignment on the computer is then used to calculate how the patient should be moved. This information is shown in the box on the lower right. (Courtesy of Best Medical, Springfield, VA, www.TeamBest.com) See COLOR PLATE 16.

The tricky part is to register the images with the planning CT (see Figure 19.35). The ultrasound transducer is at the end of an articulated arm. This arm is able to keep track of both the position and orientation of the transducer. Prior to imaging the transducer is docked at a docking station attached to the head of the linac. The position of the docking station is known with respect to the isocenter. Image information can be referenced in this way to the linac isocenter.

Chapter Summary

- **Imaging for Treatment Planning**
  (i) Plane film
  (ii) Fluoroscopy — Conventional

  (iii) CT
  (iv) MRI — 3-D & soft tissue discrimination
  (v) Ultrasound

- **Digital images** are composed of picture elements called **pixels**; radiological images are usually 512×512 pixels.

- **Gray Scale:** The number of levels of gray assigned to a pixel; this determines the contrast resolution of the image; an 8-bit gray scale has $2^8 = 256$ shades of gray.

- **CT:** Provides three-dimensional reconstruction of patient anatomy and electron density data for inhomogeneity corrections.

  —*Image reconstruction:* Need a sufficient number of projections to calculate μ for each voxel.

  —*Image size* usually 512×512 pixels; requires about 0.5 MB/slice for storage

  — $\mathrm{CT\#} = 1000\dfrac{\mu_t - \mu_w}{\mu_w}$, where μ_t is linear attenuation coefficient for tissue in a particular voxel and μ_w is the linear attenuation coefficient for water.

  —CT# sometimes called Hounsfield units (HU). CT#'s range between –1000 and +3000. For air CT# = –1000, for water CT# = 0, for dense bone 1300–1600.

  —Window and level: Level is center value of CT# displayed and window is range.

  —Modern scanners are spiral multislice units.

  —Pitch = (table travel per tube rotation)/(total length of tissue irradiated by the cone beam).

  —*Pitch < 1:* improvement in image quality but increase in dose.

  —*Diagnostic CT scanners:* Bore diameter 70 cm; concave couch top.

—*CT simulators:* Bore diameter 80 to 90 cm; flat couch top; moveable external lasers

—*Relative electron density* for patient treatment planning derived from calibration curve plot of relative electron density vs. CT#.

- **DRR:** Digitally reconstructed radiograph; simulated radiograph mathematically calculated from CT data, usually beam's-eye view for each treatment port.

- **4D CT:** Adds time dimension to the three spatial dimensions to assess or manage motion
  (1) *Prospective gated imaging:* Breath hold at either inspiration or expiration while scanning
  (2) *Retrospective/correlation imaging:* Patient breathes freely and CT slices are binned according to phase of respiratory cycle during which they were acquired.

- **MRI:** Magnetic resonance imaging uses non-ionizing RF radiation, based on magnetic properties of protons in tissue

—Magnetic field strengths of 1 to 3 T

—Contraindicated for patients with ferromagnetic implants: pacemakers, aneurism clips, etc.

—Proton precesses with Larmor frequency $\nu = \frac{\gamma B_0}{2\pi}$ (in the radio region of the spectrum), where γ is a constant called the *gyromagnetic ratio.*

—*Magnetic field gradients* used so that Larmor frequency varies with position throughout patient

—Three stages for imaging:
  (1) *Excitation:* tip direction of magnetic field of proton
  (2) *Relaxation:* magnetic field of proton returns to equilibrium with associated time scales T1 and T2
  (3) *Detection:* detect "echo" from relaxation images are weighted by spin density, T1 or T2

—MRI images are usually not used directly for treatment planning because:
  (1) They are subject to geometric distortion.
  (2) They do not provide electron density information for inhomogeneity corrections.

(3) Bone signal is weak, hard to produce useful DRRs for treatment verification.

- **Ultrasound Imaging:** Uses high-frequency sound, sound reflects off boundaries between tissues having different sound speeds.

—Speed of sound in soft tissue $c_s = 1540$ m/s; ultrasound frequency is approximately 5 MHz.

—*Transducer:* Converts mechanical energy to electrical energy and vice versa; used to produce and detect ultrasound.

- **PET:** Positron emission tomography; images the distribution of positron-emitting radiopharmaceutical throughout the body; metabolic imaging.

—*Coincidence detection:* Events are counted only if seen nearly simultaneously on opposite sides of ring.

—*Common radioisotope* is ^{18}F ($T_{1/2} = 110$ min), incorporated in glucose analog FDG; malignant cells exhibit enhanced glucose uptake.

—*Standard uptake volume* (*SUV*):

$$\text{SUV} = \frac{\text{Activity per unit volume / decay factor}}{\text{Injected activity / body mass}}$$

—High SUV is a sign of possible malignancy.

- **Imaging for Treatment Verification (Portal Imaging)**
  (i) Film
  (ii) Electronic portal imaging devices (EPIDs)

—A screen is used to filter out electron contamination and to provide some build-up.

—Poor quality is due to:
(1) *Poor contrast:* Predominant interaction is Compton, weak dependence on *Z*; very little differential absorption is seen compared to diagnostic films.
(2) *Scattered photons and secondary electrons:* Scattered photons are not easily removed, cannot use a grid.
(3) *Large penumbra:* Geometric + phantom scatter.

—The quality of port images degrades with increasing beam energy and patient thickness (>20 cm).

- **IGRT:** Image-guided radiation therapy; large variety of methods are used to assure correct geometric targeting:
  (1) Cone beam CT (CBCT): X-ray tube and flat-panel detector attached to linac.
  (2) MV CT: Use megavoltage beam to produce CT image: tomotherapy unit.
  (3) Ultrasound image registration for prostate treatment.
  (4) Implanted markers.

Problems

1. An axial CT image has a field of view of 250 mm in width. The image is 512×512 pixels. What is the pixel size? What is the smallest object that you are likely to be able to perceive?

2. Estimate the computer storage requirements for 100 CT axial slice images used for treatment planning. Assume that the images are 512×512, 16-bit gray scale. Give the answer in MB.

3. Estimate the time necessary to transfer these 100 CT slices over a network with a speed of 10 Mbps (megabits per second).

4. At a particular kVp, $\mu_w = 0.267\ \text{cm}^{-1}$, and for a particular sample of bone $\mu_{\text{bone}} = 0.511\ \text{cm}^{-1}$. Calculate the CT# of this bone.

5. List the following tissues in order of increasing Hounsfield number: bone, muscle, fat, lung.

6. The window and level of a CT image are chosen as +300 and +100, respectively. What CT#'s are displayed as black? What CT#'s are displayed as white?

7. A CT scanner with a 24-mm wide detector is operated at a pitch of 0.06 for a 4-D respiratory scan. How far does the table move during one tube rotation?

8. How can the quality of DRRs be improved?

9. Briefly describe the three stages in the process of MR imaging.

10. What are the contraindications for MR imaging?

11. What are the relative advantages and disadvantages of CT and MRI for treatment planning?

12. What contrast agent is frequently used in MR imaging?

13. How is the quality of portal images affected by beam energy?

14. Why do MV portal images show lower bone/soft tissue contrast than kV images?

Bibliography

Alessio, A. M., P. E. Kinahan, P. M. Cheng, H. Vesselle, and J. S. Karp. (2004). "PET/CT scanner instrumentation, challenges, and solutions." *Radiol Clin North Am* 42(6): 1017–1032.

American Association of Physicists in Medicine Report No. 24. Radiotherapy Portal Imaging Quality. Report of AAPM Task Group No. 28. New York: American Institute of Physics, 1988.

Bushong, S. C. *Radiologic Science for Technologists: Physics, Biology, and Protection,* 9th edition. St. Louis: Mosby, 2008.

Caldwell, C. B., and K. Mah. "Imaging for Radiation Therapy Planning." Chapter 2 in *The Modern Technology of Radiation Oncology,* Vol 2. J. Van Dyk (ed). Madison, WI: Medical Physics Publishing, pp. 31–89, 2005.

Caldwell, C. B., K. Mah, M. Skinner, and C. E. Danjoux. (2003). "Can PET provide the 3D extent of tumor motion for individualized internal target volumes? A phantom study of the limitations of CT and the promise of PET." *Int J Radiat Oncol Biol Phys* 55:1381–1393.

Chen, G. T. Y., C. A. Pellizzari, and E. R. M. Rietzel. "Imaging in Radotherapy." Chapter 2 in *Treatment Planning in Radiation Oncology,* 2nd edition. F. Khan (ed.), Philadelphia: Lippincott Williams and Wilkins, pp. 11–32, 2007.

Cody, D., and O. Mawlawi (Program Directors). *The Physics and Applications of PET/CT Imaging.* Proceedings of the AAPM 2008 Summer School. AAPM Medical Physics Monograph No. 33. Madison, WI: Medical Physics Publishing, 2008.

Coia, L., T. Schultheiss, and G, Hanks (eds.). *A Practical Guide to CT Simulation.* Madison, WI: Advanced Medical Publishing, 1995.

Curran, B.H., J. M. Balter, I. J. Chetty (Program Directors). *Integrating New Technologies into the Clinic: Monte Carlo and Image-Guided Radiation Therapy.* Proceedings of the AAPM 2006 Summer School. AAPM Medical Physics Monograph No. 32. Madison, WI: Medical Physics Publishing, 2006.

Goitein, M. *Radiation Oncology: A Physicist's-Eye View.* New York: Springer, 2008.

Hazle, J. D., and A. L. Boyer (eds.). *Imaging in Radiation Therapy.* Proceedings of the AAPM 1998 Summer School. AAPM Medical Physics Monograph #24. Madison, WI: Medical Physics Publishing, 1998.

Herman, M. G., J. M. Balter, D. A. Jaffray, K. P. McGee, P. Munro, S. Shalev, M. Van Herk, and J. W. Wong. (2001). "Clinical use of electronic portal imaging: report of AAPM Radiation Therapy Committee Task Group 58." *Med Phys* 28(5):712–738. Also available as AAPM Report No. 75.

Kevles, B. *Naked to the Bone: Medical Imaging in the Twentieth Century.* New York: Perseus Publishing, 1997.

McCullough, C. H., and F. E. Zink. (1999). "Performance evaluation of a multi-slice CT system." *Med Phys* 26:2223–2230.

Mutic, S. "Use of Imaging Systems for Patient Modeling PET and SPECT" in *Integrating New Technologies into the Clinic: Monte Carlo and Image-Guided Radiation Therapy.* AAPM 2006 Summer School Proceedings, AAPM Medical Physics Monograph No. 32. B. H. Curran, J. M. Balter, and I. J. Chetty, Program Directors, pp. 375–400, 2006.

Podoloff, D. A., R. H. Advani, C. Allred, A. B. Benson 3rd, E. Brown, H. J. Burstein, R. W. Carlson et al. (2007). "NCCN task force report: Positron emission tomography (PET)/computed tomography (CT) scanning in cancer." *J Compr Canc Netw* 5(Suppl. 1):S1–S23.

Van Dyk, J. (ed.). *The Modern Technology of Radiation Oncology.* Chapters 4, 5, 6, 7, and 13. Madison, WI: Medical Physics Publishing, 1999.

Van Dyk, J., and K. Mah. "Simulation and Imaging for Radiation Therapy Planning." Chapter 8 in *Radiotherapy Physics in Practice,* 2nd edition. J. R. Williams and D. I. Thwaites (eds.). Oxford, UK: Oxford University Press, 2000.

West, C. M. L., T. Jones, and P. Price. (2004). "The potential of positron-emission tomography to study anticancer-drug resistance." *Nat Rev Cancer* 4:457–469.

Index

Note: Page ranges are shown using longer dashes; an f denotes a figure; a t denotes a table.

J

K

L

N

O

P

Q

R

S